Marine Synechococcus Picocyanobacteria: Light Utilization Across Latitudes

Christophe Six, Morgane Ratin, Dominique Marie, Erwan Corre

Marine *Synechococcus* Picocyanobacteria: Light Utilization Across Latitudes

Christophe Six[1*], Morgane Ratin[1], Dominique Marie[1], Erwan Corre[2].

[1] Sorbonne Université, Centre National de la Recherche Scientifique, UMR 7144 « Adaptation et Diversité en Milieu Marin » (AD2M), group « Ecology of Marine Plankton » (ECOMAP), Station Biologique de Roscoff, 29680 Roscoff, France.

[2] Fédération de Recherche 2424, Department Analysis and Bioinformatics for Marine Science (ABiMS), Station Biologique de Roscoff, 29680 Roscoff, France.

* **To whom correspondence should be addressed**: Christophe Six, six@sb-roscoff.fr

Author contribution: C.S designed the research, analyzed the data and wrote the article. C.S. and M.R. carried out all the experimental photophysiological part. C.S. carried out the characterization of the OCPs. D.M and M.R. did the cell biovolume measurements and EC did the metagenomic part of the study.

Key words: temperature, marine *Synechococcus*, cyanobacteria, photosynthesis, orange carotenoid protein.

Abstract: The most ubiquitous cyanobacteria, *Synechococcus*, have colonized different marine thermal niches through the evolutionary specialization of lineages adapted to different ranges of temperature seawater. We used strains of *Synechococcus* temperature ecotypes to study how light utilization has evolved in function of temperature. The tropical *Synechococcus* (clade II) was unable to grow under 16°C but, at temperatures > 25°C, induced very high growth rates that relied on a strong synthesis of the components of the photosynthetic machinery, leading to a large increase in photosystem cross-section and electron flux. By contrast, the *Synechococcus* adapted to subpolar habitats (clade I) grew more slowly but was able to cope with temperatures < 10°C. We show that growth at such temperatures was accompanied by a large increase of the photoprotection capacities using the orange carotenoid protein (OCP). Metagenomic analyzes revealed that *Synechococcus* natural communities show the highest prevalence of the *ocp* genes in low temperature niches, whereas most tropical clade II *Synechococcus* have lost the gene. Moreover, bioinformatic analyzes suggested that the OCP variants of the two cold-adapted *Synechococcus* clades I and IV have undergone evolutionary convergence through adaptation of the molecular flexibility. Our study points to an important role of temperature in the evolution of the OCP. We furthermore discuss the implications of the different metabolic cost of these physiological strategies on the competitiveness of *Synechococcus* in a warming ocean. This study can help improving the current hypotheses and models aiming at predicting the changes in ocean carbon fluxes in response to global warming.

Introduction

The world ocean plays a central role in the climate regulation of the planet, in particular through the metabolic activity of the huge diversity of microorganisms it shelters. Among these, oxygenic phototrophs, i.e. phytoplankton, are responsible for major gas exchanges and carbon fluxes at global scale. Marine *Synechococcus*, the most widespread cyanobacterial genus on Earth, are extremely abundant phytoplanktonic cells thought to be responsible for a large part of the global net oceanic primary production (1). The quasi ubiquity of these picocyanobacteria relies on their current microdiversity, which results from the broad diversification of their radiation, including about 15 clades and 28 subclades (subcluster 5.1; (2, 3). Global phylogeographical studies have shown that the most prevalent *Synechococcus* lineages occupy distinct ecological niches notably defined on abiotic factors such as nutrients, light quality and temperature (see e.g. (3–7)). In particular, members of clades I and IV have been shown to dominate in cold high latitude waters, while clades II and III thrive in the warm intertropical areas. These *Synechococcus* ecotypes have different thermal *preferenda* that reflect their respective thermal niches (8, 9), showing that temperature has greatly influenced the diversification of these organisms because it constitutes a major ecological constraint on cell physiology.

Photosynthesis is considered to be among the most temperature sensitive cell processes of phototrophic organisms. Only a few studies have highlighted how, during their evolution, temperature has shaped the genomes of marine *Synechococcus*, but most of the studied processes are linked to photosynthesis. For instance, the composition of the photosynthetic membranes, the thylakoids, is highly thermoregulated through distinct physiological strategies set up by the different *Synechococcus* temperature ecotypes (10, 11). In addition, amino acid substitutions in key photosynthetic proteins have led to the diversification of protein variants that have allowed thermoadaptation of the light harvesting process (12).

The major light-harvesting system of *Synechococcus* is a giant, water soluble pigment-protein complex called the phycobilisome, which funnels light energy to photosystem II (PSII) reaction center carrying out the photosynthetic primary charge separation. The phycobilisome is composed of a central core surrounded by rods of phycobiliproteins assigned to distinct classes. While the core is always made of allophycocyanin, the rods are composed of phycocyanin and, in most marine *Synechococcus*, of two types of phycoerythrins (PE), PEI and PEII, displaying different combinations of phycobilin chromophores, depending on the strain (13–15). The phycobilisome thus constitutes the main entrance gate of light energy into the cyanobacterial cell. However, when light is excessive, *i.e.* when the rate of PSII charge separation outpaces the rate of electron utilization, the phycobilisome components are usually downregulated in order to decrease PSII light absorption cross-section,

thereby limiting the production of reactive oxygen species that can induce a lethal oxidative stress situation (16–18).

Another essential mechanism for the regulation of light utilization is the dissipation of excess light into heat. In cyanobacteria, the best studied photoprotective process of this type relies on the activity of a 3-gene operon that encodes and regulates the activity of a water-soluble, keto-carotenoid binding protein named the Orange Carotenoid Protein (OCP). This protein, discovered decades ago (19) and characterized much later (20), undergoes a photocycle whose details have been extensively studied in freshwater cyanobacteria (21–23). Upon activation by blue-green light, the carotenoid is translocated between the two globular domains and the color of the protein turns to red. The red protein binds to the phycobilisome core, intercepting light energy and inducing its thermal dissipation. OCP activity is measurable as non-photochemical quenching of chlorophyll fluorescence (NPQ), which is associated to the decrease of the energy reaching reaction centers. When light is no more excessive, the fluorescence recovery protein, encoded in the OCP operon, induces the OCP detachment from the allophycocyanin core and the dissipation stops. OCP genes are present in many phycobilisome-containing cyanobacteria genomes and three paralogous families of OCP have been described. The largest and most diverse group is the OCP1 family, which includes all the OCPs of marine *Synechococcus*. To date, OCP proteins have been well studied in freshwater cyanobacterial models but the marine OCPs, which are definitively very divergent from their freshwater counterparts (24), have never been studied.

We used a multi-scale approach including biophysics, biochemistry, genomics and ocean metagenomics to better understand how light utilization has evolved in marine *Synechococcus* across latitudes. The capacity of tuning phycobilisome light absorption versus OCP light dissipation was compared in several *Synechococcus* temperature ecotypes. This led us to study the different marine OCP variants and their global distribution in the world ocean. Our study unveils the major influence of temperature on the evolution of this protein in the oceans and sheds light on the *Synechococcus* physiological strategies involved in the response to the current global changes.

Results and discussion

Differential regulation of growth and light harvesting capacities

Synechococcus strains M16.1 (subcluster 5.1, clade II) and MVIR-18-1 (subcluster 5.1, clade I; Fig. 1A, B) have colonized contrasted thermal niches of the world ocean (3, 4, 6). M16.1 was isolated in the Gulf of Mexico where the waters reach 30°C, whereas MVIR-18-1 was isolated in the subpolar waters of the Norway sea, where the temperature is as low as 6°C in winter. The cold-adapted ecotype MVIR-

18-1, which displays higher cell biovolume (Fig. 1C), showed a moderate increase in cell size with increasing growth temperature, whereas the warm-adapted ecotype M16.1 was smaller but induced a biovolume doubling, then reaching biovolume values similar to the cold adapted strain. This cell size difference supports the so-called “temperature-size rule”, which states that there is a negative relationship between ambient temperature and organism size (25). However, these results show that the cell size of the smallest organisms can increase with growth temperature and our study suggests that this is probably linked to the regulation of light utilization and growth rate. The growth capacities of these two *Synechococcus* in our experimental conditions supported previous studies showing that they display distinct thermal *preferenda* (Fig. 1D, (8)). The tropical strain M16.1 showed optimal growth at 33°C whereas the optimal temperature was about 10°C lower for the subpolar one. The thermal limits for growth also differed drastically, with M16.1 growing from 18 to 32°C whereas MVIR-18-1 was not able to grow above 26°C but maintained measurable growth below 9°C. These two isolates, which are among the most contrasted marine *Synechococcus* thermotypes studied so far, also differed in the growth rate values they were capable of inducing. The subpolar strain never reached growth rates higher than 0.7. The tropical strain triggered very rapid growth starting from a curve shoulder at 25°C, which was the temperature at which the subpolar strain reached maximal growth before declining. These growth responses have previously been observed in other marine *Synechococcus* strains (8). This suggests that, at this temperature and in contrast to the clade I subpolar strain, the clade II tropical ecotype induced specific physiological mechanisms allowing considerable growth acceleration.

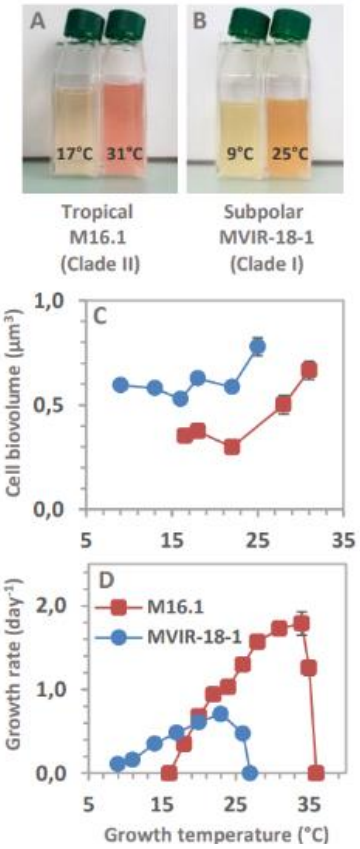

Figure 1: Culture flasks of *Synechococcus* picocyanobacteria strains M16.1 (**A**, tropical; Clade II) and MVIR-18-1 (**B**, subpolar; Clade I), grown at their thermal growth limits (cell density between 4 and 6 10^7 cells mL-1). Variations of cell biovolume (**C**) and growth rate (**D**) in *Synechococcus* spp. M16.1 (red) and MVIR-18-1 (blue), function of growth temperature, as measured by flow cytometry.

In order to better understand the mechanisms lying behind these different growth responses to temperature, we studied the relation between thermal acclimation and the regulation of photosynthesis, the major energetic process in these organisms. PAM fluorometry analyses unambiguously showed that green (540 nm) and cyan (480 nm) lights are by far the most utilized wavelengths by these cyanobacteria, in agreement with their phycoerythrobilin-rich pigment type 3a

(14), and we therefore focused our work on these wavelengths. Analysis of ETRII *vs.* irradiance curves revealed that PSII saturation irradiance E_K of the tropical strain drastically decreased at high temperature, along with an increase of the PSII efficiency α (Fig. 2A, S1, S2). In the clade I subpolar strain, these parameters varied much less. This shows that the clade II tropical strain was able of a very flexible photophysiological response, inducing efficient exploitation of the photon flux at high temperature. This was associated to an increase in chl *a* and β-carotene cell contents in both strains, which was much more pronounced in the tropical strain (Fig. 2B, C, D). As these two pigments are mostly located in the thylakoidal membranes, in the photosystem reaction centers, this suggests that acclimation to high temperature in the tropical strain induced a marked synthesis of additional thylakoid lamellas and/or photosystems, which allowed a strong increase of the rate of photosynthetic electron transport per cell. This synthesis of additional thylakoid membranes is likely associated to the marked increase in cell biovolume (Fig. 1C). Comparison of the cell content in PSII and PSI using anti-PsbD and anti-PsaC antibodies (Fig. 2E, F, S3), respectively, confirmed an enhanced photosystem biosynthesis in response to increasing growth temperature. The tropical strain M16.1, however, reached higher PSII cell contents, while the PSI cell content variations were similar between the two strains over their thermal growth range. When the data were expressed in biovolume units (Fig. S3), it could be observed that both strains have identical PSI content per μm^3 cell with a linear temperature-induced increase. However, it seems that the subpolar strain could not increase anymore the PSII content per μm^3 cell at temperatures higher than 22°C. Together with the increase in the β-carotene: chl *a* ratio in M16.1 (Fig. S4), this suggests an increase of the number of PSII relative to PSI in the tropical strain in response to increasing growth temperature, likely leading to higher trans-thylakoidal pH gradient and consequent higher ATP production (11). It will be interesting in future research to study the possible molecular differences (differential thermostability, protection by other proteins, occurrence of thermostable protein isoforms, etc.) in the photosynthetic complexes of these temperature ecotypes, in order to better understand the physiological factors that prevent/allow growth at high temperature (12).

We analyzed the light-harvesting capacities of both strains grown over their thermal *preferenda*. In response to increasing temperature, the PE cell content increased much more in the clade II tropical strain than in the clade I subpolar one, as measured by flow cytometry, spectrofluorimetry (Fig. 2G, S5A) and direct quantification of the β-subunit of the major light harvesting proteins, PEI and PEII (Fig. 2H, S3). The tropical strain reached PE cell contents twice higher than the subpolar strain, thereby giving a bright pink color to the M16.1 cultures. This shows that, in response to increasing temperature, the tropical strain drastically increased its light absorption capacities by inducing strong synthesis of PE and most probably of entire phycobilisomes, as supported by the concomitant increase of the whole

cell phycocyanin fluorescence (Fig. S5B). Consequently, while the molar PE to PSII ratio of the subpolar strain remained fairly stable at ~36 hexamers per PSII, the tropical strain increased it from 20 to 43 PE hexamers per PSII (Fig. S6). This resulted in a strong increase of the PSII absorption cross-section σ(II) at 540 and 480 nm for the tropical strain at high temperature (Figs. 2I, S7; (26)).

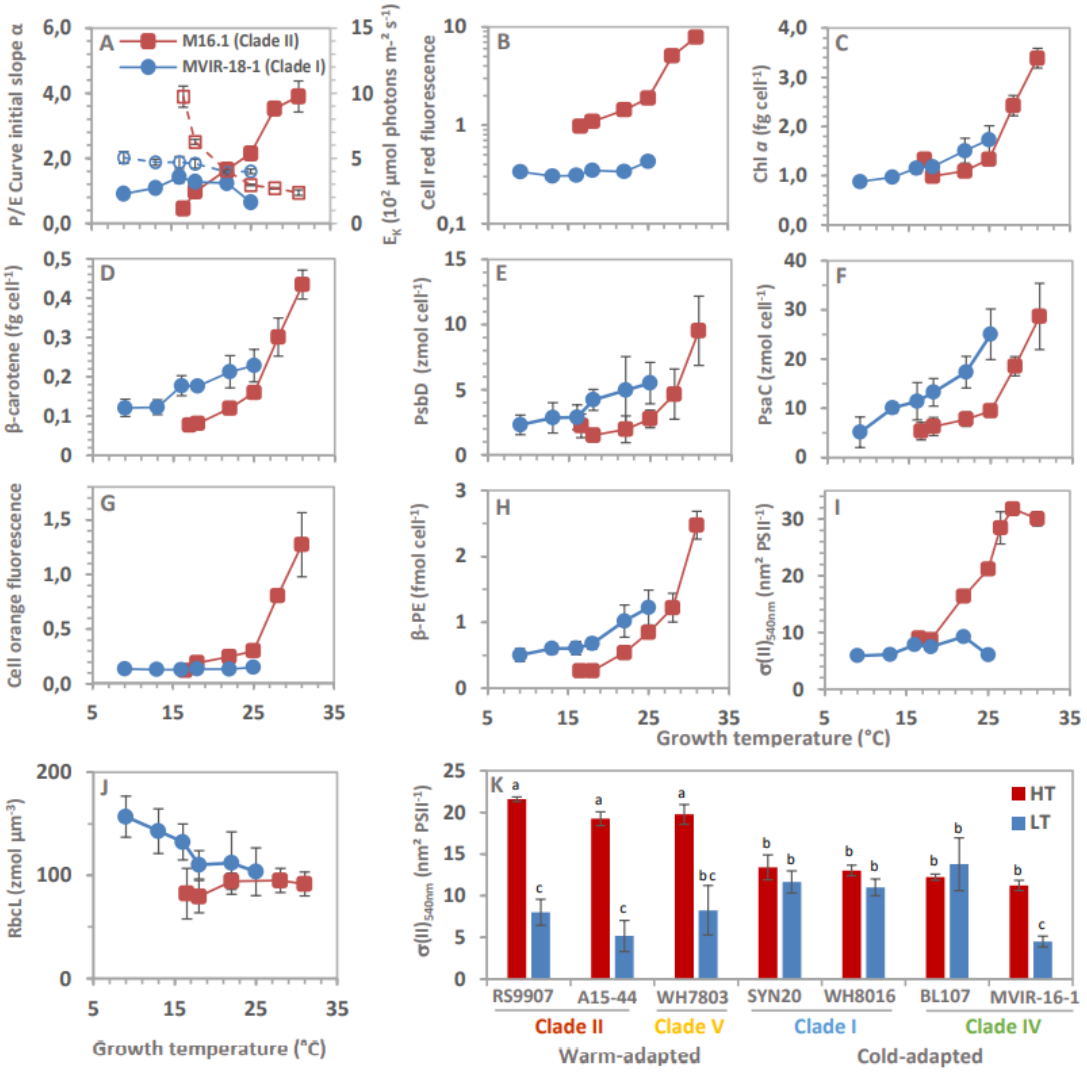

Figure 2: Variations of photophysiological parameters in the tropical M16.1 (Clade II; red) and subpolar MVIR-18-1 (Clade I; blue) *Synechococcus* strains, function of growth temperature. **A**: initial slope (α) of the electron transport vs. 540 nm irradiance curve (filled symbols), reflecting the photon dependent efficiency of photosystem II in low irradiance and saturation 540 nm irradiance (E_K) of the same curve (empty symbols), indicating the green photon flux necessary to saturate photosystem II activity. **B**: Chlorophyll *a* cellular fluorescence emitted at 680 nm as measured by flow cytometry. **C**: Chlorophyll *a* cell content as measured by high pressure liquid chromatography. **D**: β-carotene cell content as measured by high pressure liquid chromatography. **E**: Cell content in PsbD (D2), a major core protein of photosystem II, as measured by quantitative immunoblotting. **F**: Cell content in PsaC, a protein of photosystem I, as measured by quantitative immunoblotting. **G**: Phycoerythrin cellular fluorescence emitted at 525 nm as measured by flow cytometry. **H**: Cell content in β-phycoerythrin subunits (MpeB and CpeB) as measured by quantitative in-gel fluorescence. **I**: Photosystem II absorption cross-section at 540 nm, reflecting the effective size of the photosynthetic antenna. **J**: Cell biovolume content in RbcL, the large subunit of the Ribulose-1,5-bisphosphate Carboxylase Oxygenase (RuBisCO), as measured by quantitative immunoblotting. **K**: Variations of the photosystem II absorption cross-section at 540 nm in different temperature ecotypes of marine *Synechococcus* grown near their growth thermal limits. Small error bars may be hidden by the symbols. Statistics tests (Kruskal-Wallis, *df*=3, *p*-value<0.05) are represented with the letter notation.

To estimate whether this difference of response to growth temperature was specific to these two strains or a more general physiological strategy of marine *Synechococcus* cyanobacteria, we investigated the capacity to modulate σ(II) in the blue-green region in seven other phycoerythrobilin-rich *Synechococcus* strains. Among the strains we tested, those belonging to the warm-adapted clades II and V all deployed the largest effective photosynthetic antennae when grown at high growth temperature, with σ(II) being ~ 3-fold higher than at low temperature (Fig. 2K, S8). By contrast, the maximal σ(II) was significantly lower among the cold-adapted strains from clades I and IV. While clade I strains and the clade IV strain BL107 showed low or no capacities to increase σ(II) in response to high temperature, the cold-temperate clade IV strain MVIR-16-1 significantly increased σ(II) at high growth temperature. Overall, these results suggest that warm-adapted strains from clade II and V can induce very large photon absorption in response to high temperature, whereas cold-adapted strains have smaller photosynthetic antennae with strain-specific regulation capacities. There is little doubt that the ability of clade II tropical *Synechococcus* to markedly increase σ(II) and the thylakoidal components of the photosynthetic apparatus is directly linked with the capacity to considerably accelerate growth rate in response to increased temperature (8), whereas the clade I subpolar strains are unable of it.

Quantification of the Ribulose-1,5-bisphosphate Carboxylase Oxygenase (RuBisCO) enzyme, catalyzing photosynthetic carbon fixation, revealed further differences between the two strains. The tropical strain increased the RuBisCO cell content following its increase in biovolume, so that the RuBisCO content per μm^3 cell remained stable over the thermal growth range (Fig. 2J, S3). The subpolar strain showed similar RuBisCO content to the tropical one between 16 and 25°C but increased the mean RuBisCO content for temperatures lower than 16°C. Like for any enzyme, RuBisCO activity cannot be estimated using the sole protein content. It is well known that RubisCO needs to be activated by the regulatory protein RuBisCO activase, which has been shown to be temperature sensitive (27, 28). In many plants, under cold stress, the RuBisCO content is up-regulated in order to compensate for the decline of the carboxylase turnover rate (29) often induced by the RuBisCO activase activity drop. Our results thus suggest that, in the subpolar strain, the carboxylase turnover rate of the RuBisCO is significantly affected under 16°C. As the subpolar niches are the limit of the global latitudinal distribution of marine *Synechococcus*, it is possible that the specific molecular characteristics of the RuBisCO system in these cyanobacteria hinder the colonization of the colder polar niches.

Xanthophylls and temperature induced photoprotection

Marine *Synechococcus* have a simple carotenoid composition based on the CrtL-b cyclase pathway (30). From β-carotene, a few xanthophylls can be synthetized, several of which have never been identified (Fig. S9). Upon growth temperature changes, the conversion of β-carotene into β-cryptoxanthin, catalyzed by the CrtR enzyme, did not seemingly change in the two strains, since the

cell content in the two carotenoids increased similarly with increasing temperature (Fig. 2D, 3A, S10A). β-cryptoxanthin can be converted using the same enzyme into zeaxanthin, by far the most accumulated xanthophyll in all marine *Synechococcus.* Whereas in the subpolar ecotype the zeaxanthin cell content did not vary with growth temperature, it increased in the tropical strain starting from 25°C, similarly to the thylakoidal photosynthetic complexes (Fig. 3B). This led to weaker variations of the zeaxanthin to β-cryptoxanthin ratio in the MVIR-18-1 than in M16.1 (Fig. S10B), while the global zeaxanthin to chl *a* ratio decreased in the two strains following a similar rate (Fig. S10C). Although the function of zeaxanthin remains unclear in marine *Synechococcus*, this suggests that it is localized within the thylakoids.

The most interesting observation was that a part of the β-cryptoxanthin was converted in 3'-hydroxyechinenone in the clade I subpolar strain at low growth temperature, whereas this xanthophyll kept stable at low cell content in the clade II tropical strain (Fig. 3C). This reaction is catalyzed by the CrtW ketolase enzyme (Fig. S11) whose gene is part of the small OCP operon. This cyanobacterial protein generally binds 3'-hydroxyechinenone and upon blue-green light activation, interacts with the allophycocyanin phycobilisome core to dissipate light energy before it reaches the photosystem reaction center (31). This photoprotective process, which limits photosynthetic electron jamming and subsequent induction of oxidative stress, is measurable as non-photochemical quenching of chl *a* fluorescence. In order to determine whether the increase in 3'-hydroxyechinenone was associated to the induction of OCP-mediated photoprotection, we studied the capacity to induce non-photochemical quenching of PSII fluorescence under blue-green light (NPQ_{BG}), using inactinic phycobilisome-absorbed light (540 nm) and actinic OCP-absorbed light (480 nm) to monitor the energy transfer from the

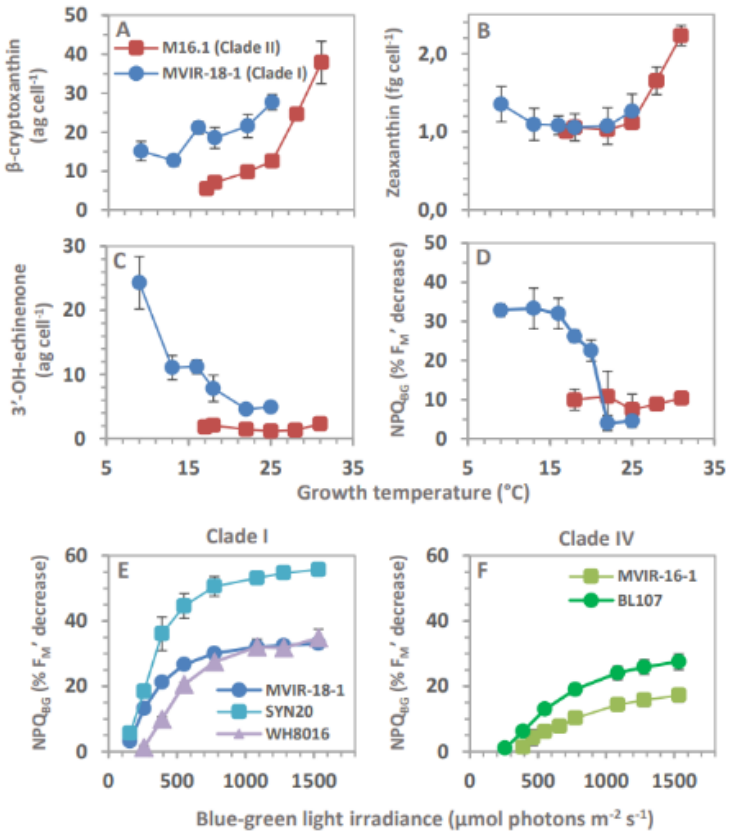

Figure 3: Variations in xanthophyll cell content and blue-green light induced non photochemical quenching of fluorescence (NPQ_{BG}) function of growth temperature. Cell content in β-cryptoxanthin (**A**), zeaxanthin (**B**) and 3'-hydroxyechinenone (**C**). **D**: Variations in NPQBG as measured by pulse amplitude modulation fluorometry, expressed in percentage of decrease of the F_M' level. Irradiance (480 nm) response curve of NPQ_{BG} in *Synechococcus* strains belonging to the subpolar clade I (**E**; blue and purple) and the cold temperate clade IV (**F**; green).

phycobilisome to the PSII (22). The results unambiguously showed that the subpolar *Synechococcus* sp. MVIR-18-1 has large NPQ_{BG} induction capacities under low growth temperature (Fig. 3D). After relaxation of the state transition process under low light, high light at 480 nm provoked a rapid drop of both the F_0 and F_M' PSII fluorescence levels, which was reversible under low light (Fig. S12). We were able to induce NPQ_{BG} only using the 440 and 480 nm wavelengths available on our fluorometer. By contrast, the tropical strain was able to induce only low and variable levels of NPQ_{BG}, which did not seem to be related to growth temperature. Considering that the OCP binds a single 3'-hydroxyechinenone molecule and using our quantitative phycobiliprotein data, we calculated that the number of OCP per allophycocyanin increased in the subpolar strain from 0.35 at 25°C to 3.4 at 9°C, which are values comparable to those reported for *Synechocystis* sp. PCC 6803 (32).

Boulay and coworkers (2008) reported NPQ_{BG} induction in four marine *Synechococcus* strains, grown at 22°C, which were all isolated from warm environments (33). This induction was however rather low, similarly to what we observed in the clade II tropical strain *Synechococcus* sp. M16.1. In addition, large scale proteomic and transcriptomic studies reported the accumulation of OCP transcripts and proteins in response to low temperature in three marine *Synechococcus* strains (9, 34). To provide insights on whether this photophysiological response is thermotype specific, we investigated the capacity of other *Synechococcus* strains to induce NPQ_{BG} in response to low growth temperature. We grew the model strain WH7803 (clade V) and 5 strains (RS9907, A15-44, RS9915, WH8102 and BOUM118) belonging to the warm-adapted clades II and III at temperatures close to the limits of their growth thermal range. Similarly to what we describe in more detail for the clade II strain M16.1 (Fig. 3D, S12), all strains belonging to clades II and III showed no or limited NPQ_{BG} induction. We also grew five other *Synechococcus* strains belonging to the two cold-adapted clades I and IV close to the limits of their thermal *preferendum*. All of them induced more or less large NPQ_{BG} in response to low growth temperature only. This suggests that the capacity to induce large NPQ_{BG} might be a feature of *Synechococcus* strains adapted to cold environments. In such thermal niches, photosynthetic organisms may undergo a slowing down of major metabolic processes, like the maintenance of the PSII complexes through the PSII repair cycle, which is partly based on the excision and replacement of non-functional D1 proteins from the PSII core (35). At low temperature, this constitutes a strongly limiting step for efficient PSII repair, as exemplified in marine diatoms (36, 37) and the green picoalga *Micromonas polaris* (38). Thus, the capacity to induce significant NPQ, protecting the cell from PSII-induced oxidative stress, may therefore be critical to maintain significant growth at low temperature.

To further characterize and compare the response of the two clades (I and IV) of cold-adapted strains, we built irradiance response curves of NPQ_{BG} in cultures all acclimated to 14°C (Fig. 3E, F). Clade I strains started inducing measurable NPQ_{BG} at 150-200 µmol photons m^{-2} s^{-1} blue-green light and the

curves saturated at irradiances higher than ~1000 µmol photons m^{-2} s^{-1}. The maximal NPQ_{BG} levels depended on the strain and were comprised between 30 and 55% of decrease of the maximal F_M' level. These characteristics are comparable to previous observations in freshwater cyanobacteria strains (33, 39, 40). Compared to clade I strains, the clade IV strains started inducing NPQ_{BG} at higher irradiances and did not show full saturation in our experimental conditions. Comparing modeled NPQ_{BG} saturation irradiance values confirmed that clade IV strains saturated NPQ_{BG} at significantly higher photon fluxes (Fig. S13). These differences of NPQ_{BG} induction between strains of the two cold-adapted clades were also visible on Ln-transformed curves, which showed that subpolar clade I strains are able to induce more NPQ_{BG} per incident photon than the cold-temperate clade IV strains (Fig. S13). These differences in OCP activity between the two cold-adapted clades are possibly related to their different, though overlapping, thermal distribution since clade IV strains inhabit slightly warmer waters than clade I.

The capacity of cold adapted strains to induce strong light dissipation at low temperature and the differences among the strains/clades can originate from a strong activation of the OCP operon, leading to a high cellular ratio of active OCP to phycobilisome, and/or from the presence of OCP variants displaying different efficiencies. Further research using purified marine OCPs and genetic transformation techniques is necessary to answer these questions.

Molecular characteristics of OCP variants

Muzzopappa and coworkers (2019) showed that marine OCPs are phylogenetically very distant from their freshwater counterparts (24), raising questions about the selective pressures at work behind this differential evolution. Using metagenomic data and recently published *Synechococcus* genomes (41), we built a database of 70 complete sequences of marine *Synechococcus* OCPs. First observations revealed that among all the known marine *Synechococcus* clades, only some of them include genomes containing the OCP operon, namely clades I, II, III, IV, V, VI, VIII, WPC1 and subcluster 5.3. The recently discovered phycobilisome-containing *Procchlorococcus* genomes do not contain the OCP operon (42). Studying the phylogenetic relationships among these protein sequences showed that the OCPs of the clade I subpolar *Synechococcus* are the most distant proteins from all other oceanic OCPs (Fig. 4A). Interestingly, the OCPs of clade IV *Synechococcus*, the other cold-adapted clade inhabiting cold temperate waters, form a sister group to the clade I subpolar OCPs. This was quite unexpected because the two cold-adapted clades I and IV have been shown to belong to two distinct taxonomic subgroups (5.1A and 5.1B) in the topology of the core phylogenies (see e.g. 2, 4, 41). Overall, these observations suggest that *ocp* genes from cold regions of the oceans have evolved differently from the others. Moreover, the fact that OCPs from *Synechococcus* clades I and IV, distant in the core phylogenies, show relatively high sequence similarity suggests an evolutionary convergence under cold temperature

selection pressure, and/or that the proteins originate from a relatively recent horizontal transfer of genes between the two cold-adapted clades.

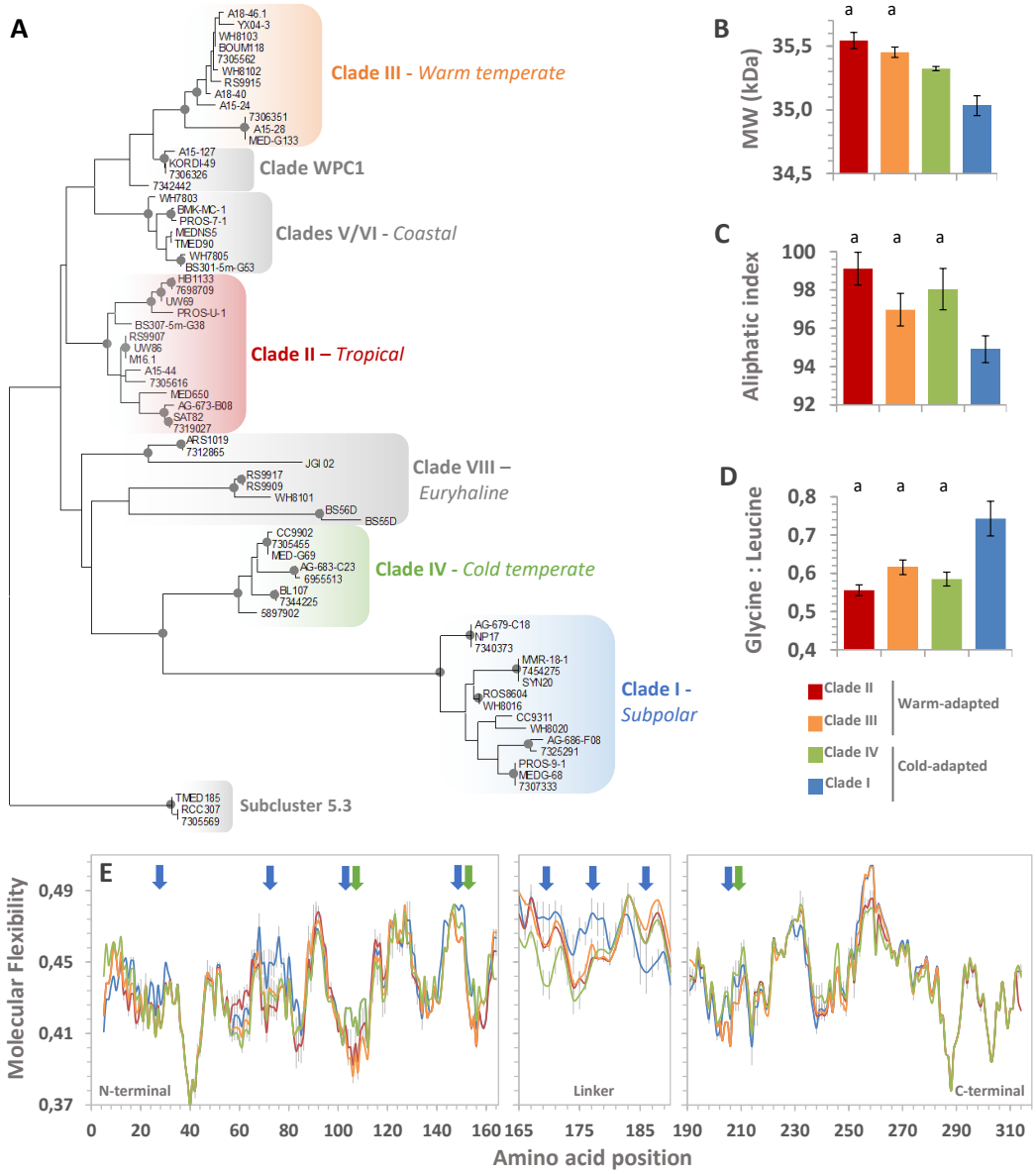

Figure 4: Molecular characteristics of orange carotenoid proteins (OCP) from marine *Synechococcus*. On the left, phylogenetic tree of OCP sequences collected in genomes and metagenomes (**A**), built using the Maximum Likelihood method (Jones-Taylor-Thornton model with gamma distribution, 500 bootstrap replications). The same tree configuration was obtained using the Neighbor Joining method (Poisson model with gamma distribution, 2000 bootstrap replications). Bootstrap values > 85 are indicated on the nodes by a grey circle. The four dominant *Synechococcus* clades are shown in colors and the minor clades, whose thermophysiology has not been yet characterized, are shown in grey. On the right, clade average molecular characteristics of OCPs from marine *Synechococcus* OCPs tropical clade II (10 sequences, red), warm temperate clade III (10 sequences; orange), cold temperate clade IV (5 sequences, green) and subpolar clade I (13 sequences, blue), including the molecular weight (**B**), the global aliphatic index (**C**) reflecting the volume of aliphatic groups, the molar glycine to leucine ratio (**D**) and the predicted average flexibility along the amino-acid sequence of the OCP linker region (**E**). Blue and green arrows show the region where clade I and Clade IV display differences in predicted molecular flexibility. Statistics tests (Kruskal-Wallis, *df*=3, *p*-value<0.05) are represented with the letter notation.

The structure of freshwater OCPs has been studied in detail (21) and most of the amino acids for which important structural functions have been evidenced are conserved in marine OCPs, with some minor substitution (39, see supplementary information). This suggests that the OCP photocycle mechanism is well conserved in marine *Synechococcus*. However, a global bioinformatic analysis of the properties of the different marine OCPs gave new insights on the evolution of this protein in the oceans. First, there is an apparent relationship between the molecular weight of the apoprotein and the thermal niche of the strains. For an equal number of amino acids, subpolar OCPs are ~500 Da lighter than the tropical ones, while temperate OCPs show intermediate molecular weights (Fig. 4B; Kruskal-Wallis, df=3, p-value<0.05). In addition, clade I OCPs are enriched in glycine, depleted in glutamine and leucine (Fig. 4C, Fig. S14) and display a lower aliphatic index, a proxy for the relative volume occupied by aliphatic side chains (Fig. 4D). OCPs from both cold-adapted clades I and IV have a higher content in serine. These differences are well known to constitute molecular adaptations to different thermal niches (44–46). For instance, a high content in the smallest amino acid glycine and a low content in hydrophobic amino acids, allow increasing the molecular flexibility of a given protein variant. In cold habitats where low temperature rigidify macromolecules, the regulation of this physical parameter is essential in order to maintain efficient activity of proteins. These conserved modifications in orthologous proteins from organisms that have evolved under different thermal environments, allow maintaining optimal physiology and provide higher fitness in a given ecological niche.

We analyzed the predicted molecular flexibility of the OCP variants (Fig.4E). The global pattern of chain flexibility was similar among OCPs but specific regions of the cold adapted OCPs showed clear differences. These proteins displayed higher flexibility in regions of the N-terminal domain, especially between residues 68 to 85, notably due to substitutions consisting in the replacement of an aspartate and a threonine at position 76 and 79, respectively, by serine residues. OCPs from the cold temperate *Synechococcus* clade IV also showed higher flexibility regions in the N- and C-terminal domains, which they share with the subpolar OCPs, in particular in the regions of residues 205 to 210 in which, notably, a serine replaces an alanine. The linker region between the two domains of the clade I subpolar OCPs displays the most different pattern of predicted flexibility. The superimposition of structural homology models of the OCP of the subpolar strain MVIR-18-1 and of the tropical strain M16.1 also clearly evidences a different conformation of the linker region (Fig. S15). During activation by blue-green light, the two domains of the OCP, which are bound by this linker, are separated in order to allow fixation on the phycobilisome (21). It is likely that this drastic conformation change of the protein, requiring high molecular flexibility of the linker region, can be impacted by low temperature. The observed modification of the flexibility of the linker of subpolar OCPs likely allows maintaining efficient activation of the OCP in the low temperature conditions prevailing in subpolar niches.

Temperature-guided evolution of OCPs in the marine Synechococcus *radiation*

Inspection of 50 genomes of marine *Synechococcus* (Cyanorak database (47) showed that, among representative strains of the four clades dominating the natural communities, the ecotypes adapted to cold and temperate environments (clades I, IV and III) all have the OCP operon, whereas it is absent in ~60% of the tropical clade II strains. This might be linked with the fact that several clade II *Synechococcus* have been shown to possess significantly smaller genomes (5), a characteristic that recalls the highly streamlined genomes of surface *Prochlorococcus*. The absence of the OCP operon in many Clade II tropical *Synechococcus* suggests that in the oceans, the OCP activity might not be essential to marine *Synechococcus* inhabiting warm and stable thermal environments.

Further examination showed that the genomic context of the OCP operon in marine *Synechococcus* genomes is relatively conserved in clades I, III and IV. However, in the genomes of the few clade II strains that have the OCP operon, the latter is surrounded by more variable genes, including unique and clade II specific genes. Furthermore, in most of these genomes, the OCP operon is contiguous to two genes involved in viral attacks and DNA insertion. The former (CK_00002022) encodes a protein harboring a PIN domain, induced during cyanophages infection (48). The second gene (CK_00033379) encodes a protein showing similarity to DNA processing chain A proteins, DprA. In many bacteria, these proteins are required for natural chromosomal and plasmid transformation and they have been proposed as new members of the recombination-mediator protein family, allowing natural bacterial transformation (49). Like the recently described tycheposons (50), these genes might constitute a hallmark of horizontal gene transfer. It is worth noting that in the other clades, these two genes are present but are associated with other gene clusters. These observations suggest that the OCP operon, in the few clade II strains that have it, could originate from a recent integration event, possibly following a more ancient quasi integral loss of the operon in the tropical clade II. The weak or absent response of the OCPs of warm adapted *Synechococcus* to high light in low temperature conditions may suggest that the OCP serves other types of acclimation responses in these cyanobacteria. For instance, although it has been less studied than the NPQ_{BG} mechanism, OCPs are known to be excellent quenchers of singlet oxygen (51). It is also possible that the OCP NPQ_{BG} in warm *Synechococcus* thermotypes is induced upon other conditions than the ones we tested in this study, for example in response to nutrient limitation.

In order to validate our hypotheses, we studied the thermal niches and the prevalence of marine OCPs in natural *Synechococcus* communities by analyzing metagenomic surface samples of 42 stations of TARA expeditions (Fig. 5A). We recruited and enumerated the different marine *Synechococcus ocp* gene variants and plotted their relative percentages against in situ seawater temperature (Fig. 5B). Subpolar Clade I *ocp* genes were present in the 6-22°C range with maximal relative abundances at

temperatures lower than 15°C. Cold-temperate Clade IV *ocp* genes were observed between 11°C and 22°C with maximal values at ~17°C. Warm-adapted clades III and II *ocp* genes were present from temperatures higher than 15°C. The relative abundance of warm temperate clade III *ocp* genes was maximal between 17°C and 25°C, at several Mediterranean stations at which clade III strains are known to dominate the *Synechococcus* communities (3, 11). The tropical clade II *ocp* genes accounted for more than 80% of the reads recruited when the seawater temperature was higher than 22°C. These thermal distributions are in agreement with the definition of the *in situ* thermal niches of the four *Synechococcus* clades (3, 4, 6), as well as the thermal *preferenda* determined experimentally on representative laboratory strains (8, 9, 11).

We studied the prevalence of each of the four *ocp* variants by calculating the ratio of the abundance of *ocp* variants in the metagenomes, to the corresponding abundance of the *petB* gene of the whole *Synechococcus* community (Fig. 5C, D, E, F, table S3). As *petB,* encoding a subunit of the cytochrome b_6/f, is a core gene present in a single copy in all *Synechococcus* genomes, this ratio reflects the probability for a *Synechococcus* genome to possess a given *ocp* gene variant. Cold-adapted *ocp* genes (clades I and IV) showed similar thermal patterns of prevalence with maximal values in their respective (overlapping) thermal niches. In the warm-adapted *Synechococcus* clade II and III, the prevalence values of the *ocp* genes were much lower than in the cold-adapted *Synechococcus*. This was particularly noticeable for the tropical clade II *ocp* genes, which were often quasi absent even at stations where clade II *Synechococcus* are known to account for more than 90% of the whole *Synechococcus* community (3). This observation strongly supports the hypothesis that many tropical Clade II *Synechococcus*, the most abundant *Synechococcus* cells in the world ocean, do not have the OCP operon. Studying in more details the intraclade prevalence of the *ocp* gene variants, i.e. the number of *ocp* sequences divided by the number of *petB* sequences for a given clade, showed that Clade II *Synechococcus* communities tend to have the *ocp* gene at the lowest temperature of the thermal distribution of this clade (< 19°C; Figure S16E).

A noticeable exception was observed for the warm-temperate clade III *Synechococcus* of the Mediterranean stations, at which the *ocp* prevalence was high. Therefore, in contrast to other regions of the Word Ocean, it seems that clade III *Synechococcus* inhabiting the Mediterranean Sea have retained the OCP operon during their evolution. Of note, this type of observation has already been reported regarding their membrane lipid metabolism (11). These genomic particularities could be interpreted as adaptive traits to the marked seasonality prevailing in the Mediterranean Sea. The OCP might indeed be useful in winter, during which the temperature can decrease down to ~12°C.

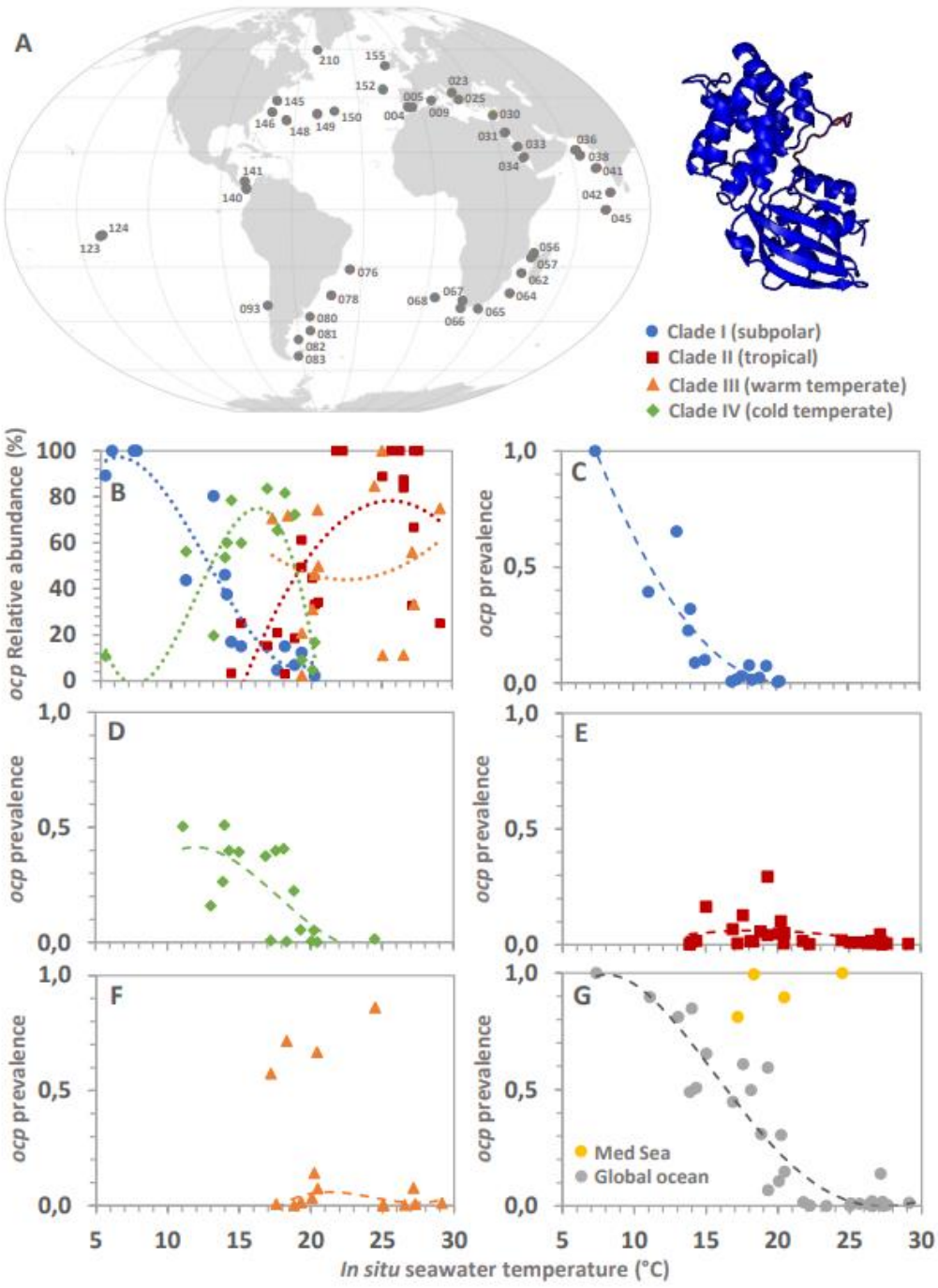

Figure 5: Metagenomic analysis of the thermal distribution of *ocp* genes from marine *Synechococcus*. **A**: Map showing the sampling stations of the TARA biosamples used in this study, and a predicted structure model of marine OCPs (see supplementary information). The relative abundance of the four dominant *ocp* gene variants (**B**), function of the seawater temperature, was expressed in percentages of the sum of the total abundance of these four genes. Values lower than 2% were excluded for better readability. The prevalence of the subpolar clade I (**C**), cold temperate clade IV (**D**), tropical clade II (**E**) and warm temperate clade III (**F**) *ocp* gene variants, function of sea water temperature, was calculated by dividing the normalized abundances of each *ocp* gene by the total abundance of the single copy core gene *petB* of all *Synechococcus* clades. The total *ocp* gene prevalence (**G**), including all known *Synechococcus* clades possessing the *ocp* gene, was calculated in the same way. Polar stations that exhibited too few reads were excluded of the analysis.

Finally, we recruited the *ocp* genes for the whole marine *Synechococcus* radiation and studied the global thermal prevalence of all *Synechococcus ocp* genes, including all the clades having the OCP operon (Fig. 5G, S16, 4A). Excluding the Mediterranean Sea stations, the *Synechococcus ocp* prevalence in the world ocean showed a clear decreasing trend from the subpolar to the highest seawater temperatures. At temperatures higher than 29°C the *ocp* gene was hardly detectable in any *Synechococcus* genome. Overall, our analysis strongly suggests that, among the *Synechococcus* lineages that have the OCP operon, the capacity to dissipate excess light as heat using the OCP is linked to the thermal niche. We also plotted the data against the seawater concentrations in nitrate, nitrite, ammonium and iron. While none of these nutrients correlated with the *ocp* prevalence (Fig. S17), suggesting that the presence of the *ocp* gene is not directly related to nutrient availability at global scale, additional observations in waters richer in nutrients could help clarify a possible role of nutrients in the capacity to dissipate excess light.

Metabolic cost of thermoacclimation in marine Synechococcus

The thermophysiological strategies we unveil in this study imply different costs of resource allocation to the photosynthetic apparatus. We retrieved from the genomes of M16-1 and MVIR-18-1 the sequences of the proteins constituting the phycobilisome, PSII, PSI and OCP and calculated the amount of amino acids, carbon, nitrogen and sulfur allocated to these pigmented protein complexes, taking in account the known stoichiometry of the protein subunits and bound chromophores (Dataset S1). Using our quantitative data and considering that a *Synechococcus* cell contains ~300 fg carbon (17, 52), we found that the pigmented protein complexes may represent up to 30% and 55% of the total carbon cell content in the clade I subpolar and clade II tropical strains we studied, respectively. This analysis revealed that, while the subpolar strain increased by 2.3-fold the cellular quota of amino acids, carbon, nitrogen and sulfur allocated to pigmented protein complexes between 9°C and 25° growth temperature, the thermal response of the tropical strain implied an ~8.5-fold increase of this material between 17°C and 31°C growth temperature. Interestingly, when the data were converted from units per cell to biovolume units, the responses became linear and we were able to determine that this corresponds to a temperature-induced increase in carbon biovolume content of 3.3 fg C μm^{-3} $°C^{-1}$ and 13.2 fg C μm^{-3} $°C^{-1}$, for the subpolar and tropical *Synechococcus* strains over their growth thermal range, respectively (Fig. S18). The capacity of clade II *Synechococcus* to rapidly allocate much resource to the photosynthetic apparatus may be interpreted as an opportunistic strategy that allows these cyanobacteria to efficiently benefit from the high temperatures that prevail in their ecological niche. In the context of a globally warming ocean, this can likely increase the competitiveness of tropical clade II *Synechococcus*, notably with respect to *Prochlorococcus* surface ecotypes which grow more slowly

(53). It is also worth noting that high abundance of *Synechococcus* have been suggested to contribute to the long-term degradation of marine food webs in shelf waters (54).

Acclimation to higher temperatures required increasing 6-fold the content in iron associated to the pigmented photosynthetic complexes, mostly due to PSI synthesis (dataset 1). However, the cellular cost in photosynthetic iron for acclimating to high temperatures was similar between the two temperature ecotypes over their whole thermal growth range. Both thermoacclimation responses were accompanied by a decrease in the C:N ratio of the pigmented protein complexes pool, which was twofold higher in *Synechococcus* sp. M16.1, indicating a higher nitrogen cost for thermoacclimation of the photosynthetic apparatus in the tropical strain (dataset 1). While the cost in carbon can be covered by a consequent increase in photosynthetic carbon fixation, this is not true for nitrogen. Marine *Synechococcus* are not diazotrophic cyanobacteria and therefore rely on dissolved sources of nitrogen, which are present at very low concentration in oligotrophic waters. Thus, our analysis suggests that the physiological strategy used by tropical *Synechococcus* to rapidly and considerably increase their growth rate with increasing temperature (Fig. 1D; 8) is probably efficient in mesotrophic areas, such as coastal waters, but might be unsuitable in oligotrophic niches. Although such analysis has never been carried out for *Prochlorococcus*, it is interesting in this context to recall that the latter picocyanobacterium has been able to colonize the warmest and most oligotrophic oceanic zones, evolving from the *Synechococcus* radiation notably by considerably decreasing the metabolic cost of its photosynthetic antenna (55).

Conclusion

Phytoplankton drives the major part of the global carbon pumping of the world ocean through the photosynthesis process. This activity is highly influenced by temperature, which constrains most enzymatic reactions such as those utilizing the photosynthetically produced ATP and NADPH molecules. The abundant and widespread marine *Synechococcus* have colonized different thermal niches through evolutionary specialization processes leading to the differentiation of lineages adapted to different temperature ranges. Here we show that the major *Synechococcus* lineages have considerably adapted their physiological strategies of light utilization to the constraints imposed by different temperature regimes. The tropical clade II *Synechococcus* are unable to grow at low temperature but, upon a temperature increase, they can rapidly develop very large capacities of light harvesting and utilization, which allow them to grow at impressive growth rates. By contrast, the *Synechococcus* adapted to subpolar niches can only moderately increase their efficiency of light utilization with increasing temperature, but are able to cope with low temperatures notably by dissipating light that cannot be used in these conditions, thereby protecting the cell from oxidative stress. For this, they use the OCP, which has evolved differently in the different marine *Synechococcus*

thermotypes. In the two phylogenetically distant cold-adapted lineages, it appears that an evolutionary convergence mechanism has adapted the OCP to cold niches notably by modifying the flexibility of the protein at certain crucial sites. By contrast, although some tropical *Synechococcus* might have gained the OCP operon through a more recent horizontal transfer, most of them have lost the OCP operon during evolution and when it is present, it provides the cell only moderate capacities of excess light dissipation with regards to temperature variations. This shows that in the oceans, temperature has been a major driver of the evolution of this important photosynthetic protein.

This study provides a prime example of the effects of the interaction of temperature with light on the evolution of important marine primary producers. One key of the evolutionary response has been the modulation of the tradeoff between light utilization and dissipation inducing, in marine *Synechococcus*, permanent modifications of the activity of the phycobilisomes (12) and the OCP in lineages that have colonized different thermal niches. We hypothesize that the opportunistic tropical clade II *Synechococcus* might become competitive phytoplankton in nitrogen-rich areas in the context of ocean warming, because they could considerably increase their efficiency of light utilization. The physiological strategies we have evidenced here can allow the improvement of the current hypotheses and models that aim at predicting the changes in carbon fluxes and food webs in the oceans in response to global warming.

Material and methods

Culture conditions and flow cytometry

Clonal *Synechococcus* strains including tropical (M16.1, RS9907, A15-44 and WH7803), warm temperate (RS9915, WH8102 and BOUM118), cold temperate (BL107 and MVIR-16-1) and subpolar (MVIR-18-1, SYN20 and WH8016) representatives, were retrieved from the Roscoff Culture Collection (table S1) and grown as previously described (12) under continuous 80 µmol photons m^{-2} s^{-1} white light supplied by multicolor LED arrays. Cultures were long-term acclimated from 9 to 35°C within temperature-controlled chambers and maintained in exponential growth phase.

Cell densities and fluorescence (excitation 488 nm, emission 525 ± 26 nm for PE and 680 ± 30 nm for chl *a*) were measured on cultures preserved within 0.25% glutaraldehyde (Sigma Aldrich, St Louis, MO, USA) using a microplate flow cytometer (Guava EasyCyte HT). Growth rates were computed as the slope of a ln(Nt) vs. time plot, where Nt is the cell concentration at time t. Biovolume measurements were carried out using a high sensitivity cytometer (Novocyte Advanteon, Agilent) equipped with two lasers at 405 and 488 nm. The cell diameter *d* was estimated by measuring the forward light scatter of the *Synechococcus* population within a range of four sizes of silica beads.

In vivo fluorimetry

Pulse Amplitude Modulation (PAM) measurements were carried out with a multi-wavelength fluorimeter Phyto-PAM II (Walz, Germany), whose cuvette holder was maintained at growth temperature.

Photosystem II quantum yield and fast kinetics – The photosystem II quantum yield F_V/F_M was measured as previously described (8) for five wavelengths (440, 480, 540, 590 or 625 nm) of modulated light. To measure the PSII cross section σ(II), dilute culture aliquots were incubated under weak far red light inducing no significant PSII excitation and oxidizing the

plastoquinone pool through PSI excitation. Single turnover pulses were triggered to record O-I_1 fast kinetics. Different pulse irradiances were tested to balance the photon dose function of the different wavelength absorption rates. The PSII cross-section $\sigma(II)_\lambda$ was calculated for each wavelength using the Phytowin 3 software (Walz, Germany; (56).

PSII electron transport vs. Irradiance curves – For each wavelength, after measurement of the basal F_0 fluorescence level, twelve steps of 90 s increasing light irradiance were applied, with measurement of the F_t and F_M' levels at the end of each step by triggering a multiple turnover saturating pulse. The PSII quantum yield under illuminated conditions was calculated as:

$$F_V'/F_M' = (F_M'-F_t)/F_M'$$

The electron transport rate ETRII (e^- $PSII^{-1}$ s^{-1}) at PSII was calculated for each step according to (56):

$$ETRII = ((F_V'/F_M') \times \sigma(II)_{\lambda nm} \times I \times 0.6022) / (F_V/F_M)$$

where I is the instantaneous irradiance at the considered step. ETRII values were plotted against instantaneous irradiance. The initial slope $\alpha_{(\lambda)}$, reflecting PSII efficiency under non saturating light, and the saturation irradiance $E_{K(\lambda)}$, where λ is the wavelength used for all light sources, were derived by fitting the photosynthesis Platt model (57).

Blue-green light induced non-photochemical quenching of fluorescence (NPQ_{BG}) - Fluorescence traces were recorded using modulated light at 540 nm, predominantly absorbed by phycoerythrobilin-rich PBS. The culture sample was acclimated to 55 µmol photons m^{-2} s^{-1} actinic blue-green light irradiance at 480 nm, then illuminated with 550 µmol photons m^{-2} s^{-1} to measure possible NPQ_{BG} induction, and then brought back under low light irradiance. During these sequences, F_M' was monitored by triggering saturating pluses. Actinic light was then turned off and when the signal was down to the F_0 level, the F_M level was measured under 550 µmol photons m^{-2} s^{-1} white light irradiance in the presence of 100 µM DCMU. When it occurred, NPQ_{BG} was expressed as the percentage of decrease of the maximal F_M' level. Light irradiance response curves for NPQ_{BG} were measured similarly, with 1 min steps of increasing 480 nm light irradiance.

Spectrofluorimetry – *In vivo* excitation spectra were recorded using a spectrofluorometer (Perkin Elmer, Waltham, MA, USA) as described in (12).

High performance liquid chromatography

Volumes of 100 mL culture were harvested in presence of 0.01% Pluronic (Sigma Aldrich) by centrifugation at growth temperature (10,000 x *g*, 10 min) and stored at -80°C until analysis. After extraction in cold 90% methanol, the extracts were injected in an HPLC 1100 Series System (Hewlett- Packard, St Palo Alto, CA, USA) equipped with a C_8 column (Waters) as described in (58). The pigment cell contents were calculated using the flow cytometry cell counts. The xanthophyll 3'-hydroxyechinenone was purified from a 5 L culture of the MVIR-18-1 strain grown at 10°C. The standard solution was quantified (59) and a calibration curve was used to quantify 3'-hydroxyechinenone in the samples.

Quantification of photosynthetic proteins by fluorescence and immunoblotting assays

Volumes of 400 mL culture were extracted according to previously described procedure (60). Protein concentration was determined by measuring absorbance at 280 nm and 0.5-4 µg protein (depending on the strain and the protein) was loaded on 4–12 % acrylamide gels, along with known quantities of standard proteins. β-PE was quantified by fluorescence in the electrophoresed gels using a LAS-4000 imager (GE Healthcare). PE-II standard proteins were obtained as described in (12). PsbD, PsaC and RbCL were quantified on PVDF membranes following a standard quantitative immunoblotting method (60). After chemoluminescence imaging, target protein concentrations were determined by fitting the sample signal on protein standard (Agrisera, Sweden).

In silico *molecular characterization of marine* Synechococcus *OCPs*

We used GeneBank, the Cyanorak information system and TARA metagenomic datasets to compile a database of 70 OCP sequences of marine *Synechococcus* (Table S2). Sequences were aligned using Bioedit 7.2.3 (61) and the maximum likelihood and neighbor-joining phylogenies were built using MEGA 10.1.8 (62). Amino-acid frequencies and physicochemical parameters were computed using ProtParam Tools (63). The molecular flexibility was studied with ProtScale. The crystal structure of *Synechocystis* sp. PCC 6803 (PDB 3MG1; (64)) was used as a template to produce homology models of the OCP of the MVIR-18-1 and M16.1 strains using Phyre² (65), then superimposed using PyMOL v1.7.4 to examine the structural differences.

Metagenomic analysis of the geographic distribution of marine OCPs

A selection of 42 sampling stations covering a wide variety of thermal niches were selected from the TARA metagenomic datasets (Table S3, (66); http://www.taraoceans-dataportal.org). Temperature and localization data for each station were retrieved from PANGAEA (https://doi.pangaea.de/10.1594/PANGAEA.840718). Metagenomic reads libraries corresponding to the surface layer and the size fraction 0.2– 1.6 µm for TARA_004 to TARA_052 and 0.2–3 µm for the other stations were selected for a total of 59 paired libraries. A selection of 33 OCP genes, retrieved from publicly accessible genomes of marine *Synechococcus* (subclusters 5.1 and 5.3) and covering all the marine OCP clades known to date, and the corresponding *petB* genes were quantified in the selected TARA marine metagenomes using the Salmon (67) quantification tools with the option «--meta» selected. Raw reads estimates were then normalized by the libraries and gene sizes before comparison.

Acknowledgments

This work was supported by the French National program EC2CO (Ecosphère Continentale et Côtière). We warmly thank Cécile Jauzein from the laboratory "Dynamiques des Ecosystèmes Côtiers" (Ifremer Brest, France) for giving access to its flow cytometer, as well as Justine Piterra for cell size microscope measurements and protein complexes representations. We are grateful to the Roscoff Culture Collection for maintaining the *Synechococcus* strains used in this study. We also acknowledge the commitment of the Tara Oceans coordinators and consortium, the Tara schooner and its captains and crew. We certify that there is no conflict of interest associated with this manuscript.

References

1. P. Flombaum, *et al.*, Present and future global distributions of the marine Cyanobacteria *Prochlorococcus* and *Synechococcus*. *Proc. Natl. Acad. Sci.* **110**, 9824–9829 (2013).
2. S. Mazard, M. Ostrowski, F. Partensky, D. J. Scanlan, Multi-locus sequence analysis, taxonomic resolution and biogeography of marine *Synechococcus*. *Environ. Microbiol.* **14**, 372–386 (2012).
3. G. K. Farrant, *et al.*, Delineating ecologically significant taxonomic units from global patterns of marine picocyanobacteria. *Proc. Natl. Acad. Sci. U. S. A.* **113**, E3365–E3374 (2016).
4. J. A. Sohm, *et al.*, Co-occurring *Synechococcus* ecotypes occupy four major oceanic regimes defined by temperature, macronutrients and iron. *ISME J.* **10**, 1–13 (2015).
5. M. D. Lee, *et al.*, Marine *Synechococcus* isolates representing globally abundant genomic lineages demonstrate a unique evolutionary path of genome reduction without a decrease in GC content. *Environ. Microbiol.* **21**, 1677–1686 (2019).
6. A. G. Kent, *et al.*, Parallel phylogeography of *Prochlorococcus* and *Synechococcus*. *ISME J.* **13**, 430–441 (2018).
7. T. Grébert, *et al.*, Light color acclimation is a key process in the global ocean distribution of *Synechococcus* cyanobacteria. *Proc. Natl. Acad. Sci. U. S. A.* **115**, E2010–E2019 (2018).
8. J. Pittera, *et al.*, Connecting thermal physiology and latitudinal niche partitioning in marine *Synechococcus*. *ISME J.* **8**, 1–14 (2014).
9. D. Varkey, *et al.*, Effects of low temperature on tropical and temperate isolates of marine *Synechococcus*. *ISME J.* **10**, 1252–1263 (2016).
10. J. Pittera, *et al.*, Thermoacclimation and genome adaptation of the membrane lipidome in marine *Synechococcus*.

Environ. Microbiol. **20**, 612–631 (2018).
11. S. Breton, *et al.*, Unveiling membrane thermoregulation strategies in marine picocyanobacteria. *New Phytol.* **225**, 2396–2410 (2019).
12. J. Pittera, F. Partensky, C. Six, Adaptive thermostability of light-harvesting complexes in marine picocyanobacteria. *ISME J.* **11**, 112–124 (2017).
13. L. J. Ong, A. N. Glazer, Phycoerythrins of marine unicellular cyanobacteria: I. Bilin types and locations and energy transfer pathways in *Synechococcus* spp. phycoerythrins. *J. Biol. Chem.* **266**, 9515–9527 (1991).
14. C. Six, *et al.*, Diversity and evolution of phycobilisomes in marine *Synechococcus* spp.: a comparative genomics study. *Genome Biol.* **8**, R259 (2007).
15. F. Humily, *et al.*, A Gene Island with Two Possible Configurations Is Involved in Chromatic Acclimation in Marine *Synechococcus*. *PLoS One* **8**, e84459 (2013).
16. S. Khorobrykh, V. Havurinne, H. Mattila, E. Tyystjärvi, Oxygen and ROS in photosynthesis. *Plants* **9**, 1–61 (2020).
17. C. Six, J. C. Thomas, B. Brahamsha, Y. Lemoine, F. Partensky, Photophysiology of the marine cyanobacterium *Synechococcus* sp. WH8102, a new model organism. *Aquat. Microb. Ecol.* **35**, 17–29 (2004).
18. C. Six, *et al.*, Two novel phycoerythrin-associated linker proteins in the marine cyanobacterium *Synechococcus* sp. strain WH8102. *J. Bacteriol.* **187**, 1685–1694 (2005).
19. T. Kay Holt, D. W. Krogmann, A carotenoid-protein from cyanobacteria. *BBA - Bioenerg.* **637**, 408–414 (1981).
20. A. Wilson, *et al.*, A Soluble Carotenoid Protein Involved in Phycobilisome-Related Energy Dissipation in Cyanobacteria. *Plant Cell* **18**, 992–1007 (2006).
21. F. Muzzopappa, D. Kirilovsky, Changing Color for Photoprotection: The Orange Carotenoid Protein. *Trends Plant Sci.* **25**, 92–104 (2020).
22. D. Kirilovsky, Photoprotection in cyanobacteria: the orange carotenoid protein (OCP)-related non-photochemical-quenching mechanism. *Photosynth. Res.* **93**, 7–16 (2007).
23. C. A. Kerfeld, M. R. Melnicki, M. Sutter, M. A. Dominguez-Martin, Structure, function and evolution of the cyanobacterial orange carotenoid protein and its homologs. *New Phytol.* **215**, 937–951 (2017).
24. F. Muzzopappa, A. Wilson, D. Kirilovsky, Interdomain interactions reveal the molecular evolution of the orange carotenoid protein. *Nat. Plants* **5**, 1076–1086 (2019).
25. A. S. Palacio, *et al.*, Changes in Population Age-Structure Obscure the Temperature-Size Rule in Marine Cyanobacteria. *Front. Microbiol.* **11**, 1–11 (2020).
26. U. Schreiber, C. Klughammer, J. Kolbowski, High-end chlorophyll fluorescence analysis with the MULTI-COLOR-PAM. I. Various light qualities and their applications. *PAM Appl. Notes* **1**, 1–21 (2011).
27. A. P. Cavanagh, D. S. Kubien, Can phenotypic plasticity in Rubisco performance contribute to photosynthetic acclimation? *Photosynth. Res.* **119**, 203–214 (2014).
28. R. F. Sage, D. A. Way, D. S. Kubien, Rubisco, Rubisco activase, and global climate change. *J. Exp. Bot.* **59**, 1581–1595 (2008).
29. J. Galmés, I. Aranjuelo, H. Medrano, J. Flexas, Variation in Rubisco content and activity under variable climatic factors. *Photosynth. Res.* **117**, 73–90 (2013).
30. C. Liang, F. Zhao, W. Wei, Z. Wen, S. Qin, Carotenoid biosynthesis in cyanobacteria: Structural and evolutionary scenarios based on comparative genomics. *Int. J. Biol. Sci.* **2**, 197–207 (2006).
31. C. Boulay, A. Wilson, D. Kirilovsky, "Orange Carotenoid Protein (OCP) Related NPQ in *Synechocystis* PCC 6803 OCP-Phycobilisomes Interactions" in *Photosynthesis. Energy from the Sun: 14th International Congress on Photosynthesis*, (2008), pp. 997–1000.
32. M. Gwizdala, A. Wilson, D. Kirilovsky, In vitro reconstitution of the cyanobacterial photoprotective mechanism mediated by the orange carotenoid protein in *Synechocystis* PCC 6803. *Plant Cell* **23**, 2631–2643 (2011).
33. C. Boulay, L. Abasova, C. Six, I. Vass, D. Kirilovsky, Occurrence and function of the orange carotenoid protein in photoprotective mechanisms in various cyanobacteria. *Biochim. Biophys. Acta - Bioenerg.* **1777**, 1344–1354 (2008).
34. U. Guyet, *et al.*, Synergic Effects of Temperature and Irradiance on the Physiology of the Marine *Synechococcus* Strain WH7803. *Front. Microbiol.* **11**, 1–22 (2020).
35. S. Takahashi, N. Murata, How do environmental stresses accelerate photoinhibition? *Trends Plant Sci.* **13**, 178–182 (2008).
36. H. Wu, S. Roy, M. Alami, B. R. Green, D. a Campbell, Photosystem II photoinactivation, repair, and protection in marine centric diatoms. *Plant Physiol.* **160**, 464–76 (2012).
37. H. Wu, A. M. Cockshutt, A. McCarthy, D. A. Campbell, Distinctive photosystem ii photoinactivation and protein dynamics in marine diatoms. *Plant Physiol.* **156**, 2184–2195 (2011).
38. G. Ni, *et al.*, Arctic *Micromonas* uses protein pools and non-photochemical quenching to cope with temperature restrictions on Photosystem II protein turnover. *Photosynth. Res.*, 1–18 (2016).
39. C. Djediat, *et al.*, Light stress in green and red Planktothrix strains: The orange carotenoid protein and its related photoprotective mechanism. *Biochim. Biophys. Acta - Bioenerg.* **1861**, 148037 (2020).
40. A. Wilson, *et al.*, A photoactive carotenoid protein acting as light intensity sensor. *Proc. Natl. Acad. Sci. U. S. A.* **105**, 12075–12080 (2008).
41. H. Doré, *et al.*, Evolutionary Mechanisms of Long-Term Genome Diversification Associated With Niche Partitioning in Marine Picocyanobacteria. *Front. Microbiol.* **11**, 1–23 (2020).
42. O. Ulloa, *et al.*, The cyanobacterium *Prochlorococcus* has divergent light-harvesting antennae and may have evolved

in a low-oxygen ocean. *Proc. Natl. Acad. Sci. U. S. A.* **118**, e2025638118 (2021).
43. R. L. Leverenz, *et al.*, A 12 Å carotenoid translocation in a photoswitch associated with cyanobacterial photoprotection. *Science (80-.).* **348**, 1463–1466 (2015).
44. B. Matthews, H. Nicholson, W. Beckte, Enhanced protein thermostability from site-directed mutations that decrease the entropy of unfolding. *Proc. Natl. Acad. Sci. U. S. A.* **84**, 6663–6667 (1987).
45. A. S. Panja, B. Bandopadhyay, S. Maiti, Protein thermostability is owing to their preferences to non-polar smaller volume amino acids, variations in residual physico-chemical properties and more salt-bridges. *PLoS One* **10**, 1–21 (2015).
46. A. S. Panja, S. Maiti, B. Bandyopadhyay, Protein stability governed by its structural plasticity is inferred by physicochemical factors and salt bridges. *Sci. Rep.* **10**, 1822 (2020).
47. L. Garczarek, *et al.*, Cyanorak v2.1: A scalable information system dedicated to the visualization and expert curation of marine and brackish picocyanobacteria genomes. *Nucleic Acids Res.* **49**, D667–D676 (2021).
48. A. Fedida, D. Lindell, Two *synechococcus* genes, two different effects on cyanophage infection. *Viruses* **9** (2017).
49. L. Huang, *et al.*, DprA is essential for natural competence in *Riemerella anatipestifer* and has a conserved evolutionary mechanism. *Front. Genet.* **10**, 1–13 (2019).
50. T. Hackl, *et al.*, Novel integrative elements and genomic plasticity in ocean ecosystems. *bioRxiv* (2020) https:/doi.org/10.1101/2020.12.28.424599.42
51. A. Sedoud, *et al.*, The cyanobacterial photoactive orange carotenoid protein is an excellent singlet oxygen quencher. *Plant Cell* **26**, 1781–1791 (2014).
52. T. M. Kana, P. M. Glibert, Effect of irradiances up to 2000 µE m-2 s-1 on marine *Synechococcus* WH7803-II. Photosynthetic responses and mechanisms. *Deep Sea Res. Part A, Oceanogr. Res. Pap.* **34**, 497–516 (1987).
53. Z. I. Johnson, et al., Niche partitioning among *Prochlorococcus* ecotypes along ocean-scale Environmental gradients. Science 311, 1737 (2006).
54. K. Schmidt, *et al.*, Increasing picocyanobacteria success in shelf waters contributes to long-term food web degradation. *Glob. Chang. Biol.* **26**, 5574–5587 (2020).
55. C. S. Ting, G. Rocap, J. King, S. W. Chisholm, Cyanobacterial photosynthesis in the oceans: The origins and significance of divergent light-harvesting strategies. *Trends Microbiol.* **10**, 134–142 (2002).
56. U. Schreiber, C. Klughammer, J. Kolbowski, Assessment of wavelength-dependent parameters of photosynthetic electron transport with a new type of multi-color PAM chlorophyll fluorometer. *Photosynth. Res.* **113**, 127–144 (2012).
57. T. Platt, C. L. Gallegos, Modelling Primary Production. In: Falkowski P.G. (eds) Primary Productivity in the Sea. Environmental Science Research, vol 19. Springer, Boston, MA. https://doi.org/10.1007/978-1-4684-3890-1_19 (1980).
58. F. Partensky, *et al.*, A novel species of the marine cyanobacterium *Acaryochloris* with a unique pigment content and lifestyle. *Sci. Rep.* **8**, 1–13 (2018).
59. S. Kosourov, G. Murukesan, J. Jokela, Y. Allahverdiyeva, Carotenoid biosynthesis in *Calothrix* sp. 336/3: Composition of carotenoids on full medium, during diazotrophic growth and after long-term H2 photoproduction. *Plant Cell Physiol.* **57**, 2269–2282 (2016).
60. F. Partensky, *et al.*, Comparison of photosynthetic performances of marine picocyanobacteria with different configurations of the oxygen-evolving complex. *Photosynth. Res.* **138(1)**, 57-71 (2018).
61. T. A. Hall, A User-Friendly Biological Sequence Alignment Editor and Analysis Program for Windows 95/98/NT. *Nucleic Acids Symp. Ser.* **41**, 95–98 (1999).
62. S. Kumar, G. Stecher, M. Li, C. Knyaz, K. Tamura, MEGA X: Molecular Evolutionary Genetics Analysis across computing platforms. *Mol. Biol. Evol.* **35**, 1547–1549 (2018).
63. E. Gasteiger, *et al.*, "Protein identification and analysis tools on the ExPASy Server" in *John M. Walker (Ed): The Proteomics Protocols Handbook*, Humana Pre, (2005), pp. 571–607.
64. A. Wilson, *et al.*, Structural determinants underlying photoprotection in the photoactive orange carotenoid protein of cyanobacteria. *J. Biol. Chem.* **285**, 18364–18375 (2010).
65. L. A. Kelley, S. Mezulis, C. M. Yates, M. N. Wass, M. E. Sternberg, The Phyre2 web portal for protein modeling, prediction and analysis. *Nat. Protoc.* **10**, 845–858 (2015).
66. S. Sunagawa, *et al.*, Structure and function of the global ocean microbiome. *Science (80-.).* **348**, 1–10 (2015).
67. R. Patro, G. Duggal, M. I. Love, R. A. Irizarry, C. Kingsford, Salmon provides fast and bias-aware quantification of transcript expression. *Nat. Methods* **14**, 417–419 (2017).

Read Me Sheet

This file has been used to study the metabolic cost of thermoacclimation in the two *Synechococcus*

The two sheets "proteins" show the calculation of the content in amino acid (AA), Carbon (C), Hydro
The complexes considered in this study were the phycobilisome (PBS), the photosystem II (PSII) rea
All these values were derived from the actual translated genomic sequences for both *Synechococcu*
For the PBS, we used the putative structural models from Six et al. (2007), i.e. a hemispherical struc
The PBS rods of M16.1 were considered to be shorter because of the absence of the gene encoding

The sheet "Comparison" uses the sheets "proteins" and our proteomic experimental data to calculate
For the PBS, the PE quantitative data were used to infer the values for a complete PBS, thanks to cc
At low temperature, the rods of the PBS of MVIR-18-1 were supposed to have lost the distal phycoer
Similarly, D1:1 was replaced by one D1:2 for calculations of the PSII values at low growth temperatu
The pigments (chlorophyll compounds and carotenoids) and the iron were included in the calculatior

The sheet "µm3" shows the conversion of the data expressed in per cell units in biovolume units.
This linearized most of the trends and allowed a fair comparison between the two strains, which have

temperature ecotypes M16.1 (tropical) and MVIR-18-1 (subpolar)

gen (H), Nitrogen (N), Oxygen (O) and Sulfur (S) of the proteins composing the pigmented photosynth
action center, the photosystem I (PSI) and the Orange Carotenoid Protein (OCP).
s strains and we used structural cristallographic studies to check the number of proteins per complex
ture including a trimeric core and six radiating rods.
the distal linker MpeC in the genome.

e the allocation in AA, C, N, S and iron (Fe) to the different complexes, function of growth temperatur
efficients calculated in the protein sheets.
ythrin (PE) hexamer, a classical stress response.
re.
ns, either from our experimental data or from predictions following published cristallographic structure

e different cell sizes.

hetic complexes

ĸ.

e.

es of the complexes.

Synechococcus sp. M16.1

Gene name Gene product	*apcA* AP alpha chain	*apcB* AP beta chain
Complex	Core	Core
Protein sequence	MSIVSNSIINAD/	MQDAITNVINK
MW (Da)	17397	17423
pI	4,76	4,89
Instability index	35	25,85
Aliphatic index	97,58	93,46
GRAVY	0,041	0,038
Ala (A)	19	21
Arg (R)	11	9
Asn (N)	3	7
Asp (D)	8	11
Cys (C)	2	2
Gln (Q)	6	4
Glu (E)	14	6
Gly (G)	17	14
His (H)	0	0
Ile (I)	11	11
Leu (L)	14	15
Lys (K)	5	5
Met (M)	6	6
Phe (F)	3	2
Pro (P)	5	3
Ser (S)	7	13
Thr (T)	8	11
Trp (W)	0	0
Tyr (Y)	8	12
Val (V)	14	10
Total AA/protein	161	162
Total AA/protein/PBS	3542	3726
Carbon C	764	763
Hydrogen H	1234	1217
Nitrogen N	208	205
Oxygen O	238	244
Sulfur S	8	8
Total atoms/protein	2452	2437

Number of Rods per PBS	6

Number of copies per PBS rod	0	0
Number of copies per PBS core	22	23
Number of copies per PBS	22	23
Number of Bilins / polypeptide	1	2
Number of Bilins / polypeptide / PBS	22	46

C atoms / protein / PBS	16808	17549
H atoms / protein / PBS	27148	27991
N atoms / protein / PBS	4576	4715
O atoms / protein / PBS	5236	5612
S atoms / protein / PBS	176	184
Total atoms / protein / PBS	53944	56051

	AP	R-PC
C atoms / phycobiliapoprotein / PBS	42026	70374
H atoms / phycobiliapoprotein / PBS	67376	111534
N atoms / phycobiliapoprotein / PBS	11524	19638
O atoms / phycobiliapoprotein / PBS	13178	22260
S atoms / phycobiliapoprotein / PBS	407	624
Total atoms / phycobiliapoprotein / PBS	134511	224430
Total AminoAcids / phycobiliapoprotein / PBS	8853	15072
Number of Bilins / phycobiliapoprotein / PBS	72	108

	AP	R-PC
Bilin C atoms / phycobiliapoprotein / PBS	2376	3564
Bilin H atoms / phycobiliapoprotein / PBS	2736	4104
Bilin N atoms / phycobiliapoprotein / PBS	288	432
Bilin O atoms / phycobiliapoprotein / PBS	432	648
Bilin S atoms / phycobiliapoprtoein / PBS	0	0
Total Bilin atoms / phycobiliapoprotein / PBS	5832	8748

C atoms / phycobiliprotein / PBS	44402	73938
H atoms / phycobiliprotein / PBS	70112	115638
N atoms / hycobiliprotein / PBS	11812	20070
O atoms / phycobiliprotein / PBS	13610	22908
S atoms / phycobiliprotein / PBS	407	624
Total atoms / phycobiliprotein / PBS	140343	233178

C atoms / full PBS	412190
H atoms / full PBS	644816
N atoms / full PBS	112012
O atoms / full PBS	126878
S atoms / full PBS	3773
Total atoms / full PBS	1299669
Total aminoacids / full PBS	82137

Allophycocyanin				
apcC	***apcD***	***apcE***	***apcF***	***rpcA***
AP linker LC	**AP alpha-B chain**	**Anchor linker LCM**	**AP beta-18 chain**	**R-PC II alpha chain**
Core	Core	Core-membrane	core	Rod base
MRLFKVTACIP	RAQCLRDYSWYL	MTVTASSGSPRVSF	MRDAISGLIGRYD	MKTPLTEAVAAADSQ
7686	18404	106224,5	19136,7	17323
9,78	5,26	9,56	4,91	5,67
46,97	35,65	41,84	37,31	23,6
70,76	87,93	78,5	106,55	77,35
-0,556	-0,177	-0,297	-0,082	-0,193
2	10	121	17	27
5	10	92	16	6
3	3	32	7	8
1	9	44	14	8
2	2	4	1	2
8	11	50	6	4
4	11	53	9	9
5	13	85	14	12
0	0	5	1	2
4	6	35	9	7
3	18	85	26	13
5	8	22	2	9
1	10	15	3	4
4	4	42	4	4
3	6	50	6	4
2	12	90	12	13
5	8	62	8	12
2	1	8	0	1
1	8	25	8	10
6	14	63	11	7
66	164	983	174	162
264	164	983	174	5832
343	809	4647	841	761
543	1301	7407	1357	1192
99	217	1381	239	206
96	247	1437	262	244
3	12	19	4	6
1084	2586	14891	2703	2409

0	0	0	0	6
4	1	1	1	0
4	1	1	1	36
0	1	1	2	1
0	1	1	2	36

1372	809	4647	841	27396
2172	1301	7407	1357	42912
396	217	1381	239	7416
384	247	1437	262	8784
12	12	19	4	216
4336	2586	14891	2703	86724

PE I	PE II	PEI+PEII	Bilin
131040	136278	267318	33
209970	218544	428514	38
37338	39576	76914	4
41352	44184	85536	6
1284	1458	2742	0
420984	440040	861024	81
28278	29934	58212	
360	444	804	

PE I	PEII	PEI+PEII
11880	14652	26532
13680	16872	30552
1440	1776	3216
2160	2664	4824
0	0	0
29160	35964	65124
		PEI+PEII
142920	150930	293850
223650	235416	459066
38778	41352	80130
43512	46848	90360
1284	1458	2742
450144	476004	926148

	Full PBS	PEI+PEII	R-PC	AP
Coefficients	**Aminoacids**	1	0,26	0,15
	C	1	0,25	0,15
	H	1	0,25	0,15
	N	1	0,25	0,15
	O	1	0,25	0,15
	S	1	0,23	0,15

R-Phycocyanin II			
rpcB	***cpcG1***	***cpcG2***	***cpeA***
R-PC II beta chain	**Rod-core linker L-RC**	**Rod-core linker L-RC**	**PEI alpha chain**
Rod base	rod-core	rod-core	medium rod
MFDAFTKVVAQAD	VAIPLLEYAPITQNSLRA(	MAIPLLGYPLSTQNGRV	MKSVVTTVVTAADA
17913	28556	28172,7	17796
5,08	8,52	5,48	5,46
35,95	33,65	49,73	24,49
91,05	84,14	79,72	82,8
0,22	-0,345	-0,301	-0,277
35	18	21	23
11	22	22	10
7	9	7	7
12	19	16	10
3	1	1	4
5	7	20	6
5	13	11	10
11	26	21	14
0	2	2	1
10	14	8	4
13	21	24	16
4	12	2	8
6	4	8	2
6	11	12	3
3	14	13	8
16	14	23	5
9	12	8	10
0	2	4	1
5	14	10	10
11	21	19	12
172	256	252	164
6192	1536	1512	11808
773	1279	1246	784
1251	2000	1931	1236
221	356	355	218
249	377	375	243
9	5	9	6
2503	4017	3916	2487
6	1	1	12
0	0	0	0
36	6	6	72
2	0	0	2
72	0	0	144
27828	7674	7476	56448
45036	12000	11586	88992
7956	2136	2130	15696
8964	2262	2250	17496
324	30	54	432
90108	24102	23496	179064

Phycoerythrin I					Phycoerythrin II
cpeB	***cpeC***	***cpeE***	***mpeA***	***mpeB***	***mpeC***
PE I beta chain	**PEI linker**	**PEI linker**	**PE II alpha chain**	**PE II beta chain**	**PEII distal linker**
medium rod	medium rod	medium rod	rod tips	rod tips	distal hexamer
MLDAFSRSVVS	MPFGPASLI	MTTATLAT PANQDRS	MKSVLTTVIGAAL	MLDAFSRQAVSA	DSSGSFIGGAQL
19028	33320	26667	17809	18644	
5,82	6,98	5,83	5,83	5,77	
32,74	46,55	40,52	25,11	41,39	
94,08	71,33	83,54	82,3	86,46	
0,215	-0,552	-0,307	-0,317	0,158	
35	21	26	22	32	
11	26	19	11	9	
8	9	15	7	12	
11	16	11	10	11	
6	3	0	3	7	
4	13	16	10	3	
7	23	13	8	5	
15	22	16	13	14	
1	5	4	1	1	
11	13	12	7	10	
14	22	20	14	13	
6	13	2	6	6	
5	4	3	2	6	
3	16	10	3	4	
3	13	8	7	3	
13	29	24	11	18	
11	12	16	10	10	
0	4	1	0	0	
6	12	9	9	5	
14	18	18	11	12	
184	294	243	165	181	0
13248	1764	1458	11880	13032	0
816	1476	1164	774	791	
1337	2285	1834	1235	1289	
237	421	342	223	231	
263	448	372	249	262	
11	7	3	5	13	
2664	4637	3715	2486	2586	0
12	1	1	12	12	0
0	0	0	0	0	0
72	6	6	72	72	0
3	0	0	3	3	1
216	0	0	216	216	0
58752	8856	6984	55728	56952	0
96264	13710	11004	88920	92808	0
17064	2526	2052	16056	16632	0
18936	2688	2232	17928	18864	0
792	42	18	360	936	0
191808	27822	22290	178992	186192	0

mpeE PEII linker	*mpeD* PEI-PEII linker
rod tips	PEI-PEII junction
MPALKYKR	MSASQGFGAASLNDAPVSFSRTRNA
30901	59180
8,93	8,3
33,83	35,7
66,33	69,58
-0,202	-0,377
38	72
13	45
12	27
12	22
4	3
11	23
11	33
29	47
7	11
10	22
19	35
15	12
8	12
18	26
9	22
28	56
18	30
0	1
13	19
14	30
289	548
1734	3288
1364	2569
2106	4030
380	768
418	814
12	15
4280	8196

1	1
0	0
6	6
1	1
6	6

8184	15414
12636	24180
2280	4608
2508	4884
72	90
25680	49176

Gene name	***psbAI***
Gene product	**D1.1**
Complex	RCII
Protein sequence	MLVFQAEH
MW (da)	39434
pI	5,5
Instability index	36,37
Aliphatic index	88388
GRAVY	0,289
Ala (A)	36
Arg (R)	13
Asn (N)	22
Asp (D)	8
Cys (C)	5
Gln (Q)	13
Glu (E)	15
Gly (G)	34
His (H)	10
Ile (I)	25
Leu (L)	31
Lys (K)	1
Met (M)	13
Phe (F)	27
Pro (P)	16
Ser (S)	29
Thr (T)	14
Trp (W)	10
Tyr (Y)	14
Val (V)	22
Total Amino Acid	358
Carbon C	1808
Hydrogen H	1683
Nitrogen N	463
Oxygen O	497
Sulfur S	18
Total atoms	4469

Total Amino Acid / RCII	3352
Protein Carbon C / RCII	16669
Protein Hydrogen H / RCII	24431
Protein Nitrogen N / RCII	4321
Protein Oxygen O / RCII	4699
Protein Sulfur S / RCII	117
Total protein atoms / RCII	50237

Stress PSII includes a D1:2 protein

Total Amino Acid / RCII	3353
Protein Carbon C / RCII	16675
Protein Hydrogen H / RCII	25436
Protein Nitrogen N / RCII	4316
Protein Oxygen O / RCII	4698
Protein Sulfur S / RCII	114

Total protein atoms / RCII	51239

psbAII D1.2	*psbB* CP47	*psbC* CP43	*psbD* D2	*psbE* alpha cyt b559	*psbF* beta cyt b559	*psbH* PsbH	*psbI* PsbI
RCII	RCII	RCII	RCII	RCII	RCII	RCII	RCII
MLVFQAEI	MALYELA	VVTLSNI	MTIAVGF	MAAGSTGERPFFE	MTQAPPVATTPRI	MAQRTRLGDI	MLALKISVYS
39239	53325	50587	39249	9091	5186	7390,9	4414
5,38	5,33	6,32	5,35	6,55	12	9,52	5,92
38,84	35,77	32,14	41,36	29,93	42,16	31,27	25,97
91,34	77,62	89,55	93,45	85,73	99,78	132,73	104,9
0,357	-0,002	0,211	0,391	0,118	0,522	0,611	0,674
40	49	39	37	9	6	1	2
12	25	20	15	5	4	33	2
20	12	20	13	0	1	5	0
7	26	16	10	3	0	1	3
3	1	2	3	0	0	0	0
12	15	11	11	2	2	2	0
16	25	17	18	5	0	2	1
34	57	63	33	6	2	8	2
10	12	12	8	1	1	0	0
20	25	28	19	6	3	4	2
33	37	48	40	6	5	13	5
1	12	9	4	3	0	2	2
12	12	15	10	1	2	3	1
27	42	33	35	7	4	3	6
16	31	24	16	5	5	3	2
27	18	25	17	8	0	2	5
16	27	21	19	5	6	3	1
10	15	17	14	1	1	2	0
15	13	15	8	4	1	2	1
28	29	27	21	5	3	7	4
359	483	462	351	82	46	96	39
1814	2464	2343	1842	421	244	345	210
2688	3640	3491	2712	639	380	550	319
458	636	603	454	105	64	86	47
496	671	621	476	118	57	87	55
15	13	17	13	1	2	3	1
5471	7424	7075	5497	1284	747	1071	632

Reaction Center II							
psbJ **PsbJ**	***psbK*** **PsbK**	***psbL*** **PsbL**	***psbM*** **PsbM**	***psbN*** **PsbN**	***psbO*** **PsbO**	***psbP*** **CyanoP**	***psbQ*** **CyanoQ**
RCII	RCII	RCII	RCII	RCII	RCII	RCII	RCII
MSGKKSPYPI	MAAFTLDLLA	MERNPNPN	METNDLGFVA	VMETSSPALS	MRIRPLLAVV	MARGLIAPLM	MLKALSRLAA
7058	5268	4508	3740	4882	29685	21103	16286
9,39	4,03	5,9	3,57	3,85	4,61	5,23	6,59
53,8	39,43	33,16	15,07	42,94	32,2	40,51	37,69
73,79	141,28	99,74	149,12	91,28	76,67	106,53	98,45
0,033	1,247	0,241	1,138	0,366	-0,293	0,039	-0,067
5	7	0	3	5	19	17	25
4	1	2	0	0	13	16	12
1	0	6	3	0	8	6	4
3	2	0	1	5	20	10	11
0	0	0	0	0	4	3	2
0	3	0	1	1	11	6	5
1	1	2	2	2	19	15	9
10	1	2	2	5	30	17	5
0	0	0	0	1	2	5	1
1	3	0	4	1	15	6	4
5	10	7	6	5	21	26	21
2	0	0	0	1	12	2	8
2	1	2	1	1	4	3	4
3	6	4	3	4	13	4	6
7	4	3	1	4	12	5	5
5	2	3	1	4	22	12	12
4	1	2	2	2	24	11	2
3	1	0	0	0	0	2	1
3	1	2	1	1	9	5	3
7	3	4	3	5	18	22	8
66	47	39	34	47	276	193	148
326	259	208	176	223	1299	926	718
490	390	317	276	335	2044	1493	1164
84	54	51	38	51	350	267	204
88	61	57	49	70	429	284	215
2	1	2	1	1	8	6	6
990	765	635	540	680	4130	2976	2307

psbT	*psbU*	*psbV*	*psbX*	*psbY*	*psbZ*	*psb28*
PsbT	**PsbU**	**cyt c-550**	**PsbX**	**PsbY**	**Ycf9**	**Psb29**
RCII	RCII	RCII	RCII	RCII	RCII	RCII
MESFAYVLII	MKRLLSWLTC	VLIGLAVISI	MTPSLSNFLS	MDLRLVLVAS	MQFINTLTVI	MSKAAIQFFR
3458	15007	16106	4331	4334	6651	14200,61
8,25	4,89	4,39	5,71	12	5,82	4,56
22,84	35,39	35,47	18,45	65,45	32,6	38,55
126,13	87,41	82,67	141,25	146,5	155,48	50,79
1,068	-0,375	-0,205	0,87	0,863	1,427	-0,675
5	10	17	2	7	7	14
1	10	6	1	4	2	10
0	7	4	1	1	3	5
1	15	15	2	1	1	9
0	0	2	0	0	0	0
0	5	3	2	2	1	10
1	4	8	0	0	1	11
1	11	13	2	3	3	11
0	0	3	0	0	0	0
4	6	7	3	3	3	4
4	15	13	8	8	11	3
2	6	5	1	1	0	3
1	5	4	1	2	1	6
4	4	3	2	1	4	8
2	6	9	2	1	1	4
1	10	9	6	2	7	8
2	5	11	2	0	2	8
0	1	2	1	1	2	2
1	6	6	0	0	1	3
1	9	10	4	3	12	8
31	135	150	40	40	62	127
168	658	707	200	197	315	612
262	1046	1100	326	335	500	939
36	184	188	48	57	74	177
40	207	230	56	48	81	202
1	5	6	1	2	1	6
507	2100	2231	631	639	971	1936

Gene name	*psaA*	*psaB*	*psaC*	*psaD*
Gene product	PsaA	PsaB	PsaC	PsaD
Complex	RCI	RCI	RCI	RCI
Protein sequence	MTISPPEI	MATKFPS	MSHAVKI	LNGQLPÇ
MW (da)	83578,9	81834,5	8842,2	15405
pI	6,76	6,39	5,15	8,73
Instability index	22,89	25,95	51,06	40,28
Aliphatic index	94,07	89,96	72,22	66,52
GRAVY	0,268	0,171	0,026	-0,659
Ala (A)	94	79	6	10
Arg (R)	20	17	5	8
Asn (N)	31	31	0	10
Asp (D)	33	28	6	4
Cys (C)	3	4	9	1
Gln (Q)	30	25	2	6
Glu (E)	14	21	4	11
Gly (G)	75	70	6	14
His (H)	44	42	1	3
Ile (I)	54	44	4	7
Leu (L)	66	76	5	11
Lys (K)	21	20	3	9
Met (M)	23	18	3	3
Phe (F)	49	51	1	7
Pro (P)	30	30	4	8
Ser (S)	49	46	5	6
Thr (T)	32	38	7	10
Trp (W)	26	29	1	1
Tyr (Y)	18	28	3	5
Val (V)	55	40	6	4
Total Amino Acid	767	737	81	138
Carbon C	3851	3809	374	682
Hydrogen H	5765	5587	600	1064
Nitrogen N	1023	977	104	194
Oxygen O	1022	1004	119	206
Sulfur S	26	22	12	4
Total atoms	11687	11399	1209	2150

Total Amino Acid / RCI	2311
Protein Carbon C / RCI	11605
Protein Hydrogen H / RCI	17494
Protein Nitrogen N / RCI	3036
Protein Oxygen O / RCI	3129
Protein Sulfur S / RCI	86
Total protein atoms / RCI	35350

Reaction Center I						
psaE	***psaF***	***psaI***	***psaJ***	***psaK***	***psaL***	***psaM***
PsaE	**PsaF**	**PsaI**	**PsaJ**	**PsaK**	**PsaL**	**PsaM**
RCI	RCI	RCI	RCI	RCI	RCI	RCI
MAITRGAKV	MRRLFAVVL	MTGDFAAA\	MNKFLTAAF	MLTHLFAIAF	MTVTPAADF	MAPMETVLSAPEVFIALV\
7590,2	17067,67	3974,8	4351,2	8514,3	17336	3868,65
6,17	8,84	4,37	6,51	10,32	6,02	4,75
17,53	28,96	22,18	40,14	20,41	22,73	27,01
81,88	86,68	136,05	102,89	126,35	94,6	147,84
-0,243	0,169	1,592	0,816	1,056	0,371	1,346
6	26	7	6	14	17	9
5	10	1	1	1	4	1
5	1	0	2	3	9	0
2	7	1	1	0	4	0
0	3	0	0	1	4	0
1	5	0	0	1	5	0
6	7	1	1	0	4	3
7	13	3	1	11	20	0
0	2	0	1	4	2	1
5	7	5	3	8	8	2
2	14	2	4	10	19	6
3	7	0	1	3	3	0
1	3	1	2	4	1	2
3	10	4	5	3	11	1
3	7	3	3	4	14	2
4	11	0	0	5	5	3
4	7	3	3	4	12	1
1	3	1	2	1	4	0
3	5	0	0	0	6	1
8	10	6	2	8	11	5
69	158	38	38	85	163	37
338	774	193	211	389	806	178
530	1200	298	310	636	1212	292
94	208	42	48	104	200	42
103	216	46	48	99	217	49
1	6	1	2	5	5	2
1066	2404	580	619	1233	2440	563

	OCP
	ocp
	Ocp
	OCP
/AAHAAVLALRLSISLYEA	MFTLDKARQIFPDTLTADAVPAITARFKLLSAEDQLALIWFAYLEMG
	35562,2
	4,74
	31,61
	99,12
	0,036
	32
	12
	13
	21
	3
	19
	19
	19
	0
	22
	35
	18
	10
	19
	19
	10
	13
	5
	8
	21
Total Amino Acid / OCP	318
Carbon C / OCP	1621
Hydrogen H / OCP	2535
Nitrogen N / OCP	409
Oxygen O / OCP	462
Sulfur S / OCP	13
atoms / OCP	5040

QTITVAAPGAARMELARPILDQILAMSFDEQTKVMCDLAAKINSPISSTYAYWSVNVKLCFWYELGEYMRQGK

VAPIPQGYKLSANANSVLEAVKKVEQGQQITLLRNFVVDMGFDPNIDDDKIVAEPIVAPTPVEEREEIFIPGVLNQ

QTILSYMQLLNANDFDQLIDLFLDDGALQPPFQRPIVGREAILKFFKRDCQNLKLMPQGGFGEPAEGGFNQIKV

TGKVQTPWFGREVGMNVAWRFLLDENDKIYFVAIDLLASPAELLKLGAK

Synechococcus sp. MVIR-18-1

Gene name	*apcA*	*apcB*
Gene product	AP alpha chain	AP beta chain
Protein sequence	MSIVSNSIINAD/	MQDAITNVINK
MW (Da)	17466,8	17,514
pI	4,76	4,84
Instability index	43,36	25,21
Aliphatic index	92,67	93,4
GRAVY	-0,037	0,012
Complex	Core	Core
Ala (A)	15	17
Arg (R)	12	7
Asn (N)	3	8
Asp (D)	8	11
Cys (C)	1	2
Gln (Q)	5	5
Glu (E)	14	5
Gly (G)	17	13
His (H)	0	0
Ile (I)	11	11
Leu (L)	13	16
Lys (K)	4	6
Met (M)	6	6
Phe (F)	4	2
Pro (P)	5	3
Ser (S)	13	14
Thr (T)	8	14
Trp (W)	0	0
Tyr (Y)	8	12
Val (V)	14	10
Total AA/protein	161	162
Total AA/protein/PBS	3542	3726
Carbon C	765	768
Hydrogen H	1229	1226
Nitrogen N	209	202
Oxygen O	243	248
Sulfur S	7	8
Total atoms/protein	2453	2452

Number of Rods per PBS	6

Number of copies per PBS rod	0	0
Number of copies per PBS core	22	23
Number of copies per PBS	22	23
Number of Bilins / polypeptide	1	2
Number of Bilins / polypeptide / PBS	22	46

C atoms / protein / PBS	16830	17664
H atoms / protein / PBS	27038	28198
N atoms / protein / PBS	4598	4646
O atoms / protein / PBS	5346	5704
S atoms / protein / PBS	154	184
Total atoms / protein / PBS	53966	56396

	AP	R-PC
C atoms / phycobiliapoprotein / PBS	42181	70524
H atoms / phycobiliapoprotein / PBS	67513	111654

N atoms / phycobiliapoprotein / PBS	11475	19650
O atoms / phycobiliapoprotein / PBS	13368	22470
S atoms / phycobiliapoprotein / PBS	385	612
Total atoms / phycobiliapoprotein / PBS	134922	224910
Total AminoAcids / phycobiliapoprotein / PBS	8839	15060
Number of Bilins / phycobiliapoprotein / PBS	72	108

	AP	**R-PC**
Bilin C atoms / phycobiliapoprotein / PBS	2376	3564
Bilin H atoms / phycobiliapoprotein / PBS	2736	4104
Bilin N atoms / phycobiliapoprotein / PBS	288	432
Bilin O atoms / phycobiliapoprotein / PBS	432	648
Bilin S atoms / phycobiliapoprtoein / PBS	0	0
Total Bilin atoms / phycobiliapoprotein / PBS	5832	8748

C atoms / phycobiliprotein / PBS	44557	74088
H atoms / phycobiliprotein / PBS	70249	115758
N atoms / hycobiliprotein / PBS	11763	20082
O atoms / phycobiliprotein / PBS	13800	23118
S atoms / phycobiliprotein / PBS	385	612
Total atoms / phycobiliprotein / PBS	140754	233658

C atoms / full PBS	482533
H atoms / full PBS	755353
N atoms / full PBS	131199
O atoms / full PBS	149118
S atoms / full PBS	4399
Total atoms / full PBS	1522602
Total aminoacids / full PBS	97633

A reduced PBS misses the distal PEII hexamer on each rod

C atoms / reduced PBS	471837
H atoms / reduced PBS	738153
N atoms / reduced PBS	128111
O atoms / reduced PBS	145648
S atoms / reduced PBS	4289
Total atoms / reduced PBS	1488038
Total aminoacids / reduced PBS	95034

Allophycocyanin				
apcC	*apcD*	*apcE*	*apcF*	*rpcA*
AP linker LC	AP alpha-B chain	Anchor linker LCM	AP beta-18 chain	R-PC II alpha chain
MRLFKVTACIPSPI	MSVVRDLILKADD	MTVTASSGSPRVSF	MRDAITGLIGRYD	MKTPLTEAVAAADSQ
7714	18315	105943	19430	17365
10,03	5,54	9,51	5,09	5,66
52,95	43,15	44,5	42,74	24,61
70,76	87,99	80,37	98,16	72,47
-0,573	-0,21	-0,337	-0,167	-0,276
Core	Core	Core-membrane	core	Rod base
2	12	94	15	23
6	12	92	18	6
3	3	31	5	8
0	9	44	15	7
2	2	5	3	2
7	11	50	4	5
5	10	56	10	9
5	12	82	13	13
0	0	3	1	2
4	5	36	9	6
3	20	92	25	13
5	6	26	3	8
1	8	12	5	4
4	4	44	5	4
3	6	56	6	6
3	16	86	13	13
4	7	63	8	15
2	1	6	0	1
1	8	27	8	10
6	12	64	8	7
66	164	969	174	162
264	164	969	174	5832
344	802	4660	849	762
547	1289	7432	1368	1190
101	221	1364	242	206
95	248	1427	263	246
3	10	17	8	6
1090	2570	14900	2730	2410

0	0	0	0	6
4	1	1	1	0
4	1	1	1	36
0	1	1	2	1
0	1	1	2	36

1376	802	4660	849	27432
2188	1289	7432	1368	42840
404	221	1364	242	7416
380	248	1427	263	8856
12	10	17	8	216
4360	2570	14900	2730	86760

PE I	PE II	PEI+PEII	Bilin
130872	199158	330030	33
210198	320160	530358	38

37638	57612	95250	4
41466	64578	106044	6
1362	2040	3402	0
421536	643548	1065084	81
28284	45450	73734	
360	666	1026	

PE I	PEII	PEI+PEII
11880	21978	33858
13680	25308	38988
1440	2664	4104
2160	3996	6156
0	0	0
29160	53946	83106
		PEI+PEII
142752	221136	363888
223878	345468	569346
39078	60276	99354
43626	68574	112200
1362	2040	3402
450696	697494	1148190

	Full PBS	PEI+PEII	R-PC	AP
Coefficients	**Aminoacids**	1	0,20	0,12
	C	1	0,20	0,12
	H	1	0,20	0,12
	N	1	0,20	0,12
	O	1	0,21	0,12
	S	1	0,18	0,11

	Reduced PBS	PEI+PEII	R-PC	AP
Coefficients	**Aminoacids**	1	0,25	0,15
	C	1	0,24	0,15
	H	1	0,24	0,15
	N	1	0,24	0,14
	O	1	0,25	0,15
	S	1	0,22	0,14

R-Phycocyanin II			Phycoerythrin	
rpcB	*cpcG1*	*cpcG2*	*cpeA*	*cpeB*
R-PC II beta chain	Rod-core linker L-RC	Rod-core linker L-RC	PEI alpha chain	PE I beta chain
MFDAFTKVVAQAD	VAIPLLQYAPITQNSRVA	MTIPVLTYSQKSQNSRV	MKSVVTTVVTAADA	MLDAFSRSVVS
17928	28319	28912,9	17736	19157,8
5,06	9,01	8,47	5,45	6,56
37,87	39,36	39,01	28,92	37,57
91,57	82,09	79,72	83,41	89,73
0,177	-0,34	-0,313	-0,191	0,052
Rod base	rod-core	rod-core	medium rod	medium rod
31	19	11	25	26
11	22	22	11	13
9	7	10	5	8
11	18	13	11	13
3	1	2	4	6
5	8	13	6	3
5	11	15	9	6
12	23	21	13	20
0	2	1	1	1
11	15	19	4	11
14	20	18	15	15
3	11	8	7	6
5	4	11	3	5
6	11	12	3	3
3	14	7	6	4
19	19	24	9	14
9	12	14	8	11
0	2	4	1	0
5	16	12	10	6
10	18	16	13	13
172	253	253	164	184
6192	1518	1518	11808	13248
772	1271	1279	777	818
1248	1977	2004	1228	1340
222	351	356	218	242
252	374	383	243	265
8	5	13	7	11
2502	3978	4035	2473	2676

6	1	1	12	12
0	0	0	0	0
36	6	6	72	72
2	0	0	2	3
72	0	0	144	216

27792	7626	7674	55944	58896
44928	11862	12024	88416	96480
7992	2106	2136	15696	17424
9072	2244	2298	17496	19080
288	30	78	504	792
90072	23868	24210	178056	192672

n I		Phycoerythrin II				
cpeC	***cpeE***	***mpeA***	***mpeB***	***mpeC***	***mpeE***	***mpeD***
PEI linker	**PEI linker**	**PE II alpha chain**	**PE II beta chain**	**PEII distal linker**	**PEII linker**	**PEI-PEII linker**
MPFGPASLI	MSQPLTLAT	MKSVITTVVGSAI	MLDAFSRKAVSA	MLGAETSLKSLTS	MVAIKPTRI	MDTNQASSGFG
33394	26888	17630,8	18356	32184	30446	59671
8,69	9,54	6,57	6,55	8,92	9,32	8,82
41,17	32,6	22,63	34,95	41,49	38,71	35,91
78,3	79,55	82,91	87,51	67,95	60,43	69,69
-0,511	-0,41	-0,236	0,204	-0,471	-0,523	-0,391
medium rod	medium rod	rod tips	rod tips	distal hexamer	rod tips	PEI-PEII junction
21	15	24	31	255	21	59
27	12	10	9	17	16	39
8	14	9	9	15	14	20
15	7	10	11	10	10	24
2	0	3	7	2	5	6
12	12	8	1	16	8	25
23	14	7	5	16	17	32
22	23	14	18	23	22	45
3	5	1	1	6	6	11
15	16	7	9	11	12	27
26	21	13	14	21	12	32
14	17	7	7	13	21	23
3	6	3	4	6	6	9
13	9	3	4	14	15	27
13	5	5	3	18	10	22
27	24	12	19	28	30	61
14	21	8	11	21	21	32
4	1	0	0	0	1	3
15	10	9	5	14	11	19
17	12	12	13	17	18	32
294	244	165	181	523	276	548
1764	1464	17820	19548	3138	1656	3288
1488	1184	764	782	1420	1334	2611
2323	1894	1221	1277	2212	2092	4092
419	334	221	227	400	380	758
447	368	246	259	440	415	818
5	6	6	11	8	11	15
4682	3786	2458	2556	4480	4232	8294

1	1	18	18	1	1	1
0	0	0	0	0	0	0
6	6	108	108	6	6	6
0	0	3	3	1	1	1
0	0	324	324	6	6	6

8928	7104	82512	84456	8520	8004	15666
13938	11364	131868	137916	13272	12552	24552
2514	2004	23868	24516	2400	2280	4548
2682	2208	26568	27972	2640	2490	4908
30	36	648	1188	48	66	90
28092	22716	265464	276048	26880	25392	49764

	Gene name	*psbAI*	*psbAII*	*psbB*	*psbC*	*psbD*
	Gene product	D1.1	D1.2	CP47	CP43	D2
AESKWNKPVSF	Protein sequence	MLVFQAEH	MLVFQAEH	ATPVELTCIFGGIAAIFRFL		
	MW (da)	39370	39301	57297	50753	39323
	pI	5,71	5,38	5,68	6,06	5,35
	Stability	36,23	38,76	32,85	32,86	43,77
	Aliphatic index	90,73	89,13	82,94	90,19	93,16
	GRAVY	0,324	0,305	0,06	0,218	0,376
	Complex	RCII	RCII	RCII	RCII	RCII
	Ala (A)	33	38	50	40	35
	Arg (R)	13	12	28	20	15
	Asn (N)	22	21	12	21	13
	Asp (D)	9	7	25	16	10
	Cys (C)	4	3	1	2	2
	Gln (Q)	11	13	11	12	11
	Glu (E)	13	16	27	18	18
	Gly (G)	35	35	63	60	33
	His (H)	11	10	15	12	8
	Ile (I)	20	20	27	31	20
	Leu (L)	34	32	44	47	40
	Lys (K)	1	1	12	8	4
	Met (M)	14	12	12	14	11
	Phe (F)	26	27	40	35	35
	Pro (P)	15	16	34	23	16
	Ser (S)	29	25	20	24	19
	Thr (T)	16	18	30	23	19
	Trp (W)	10	10	17	16	14
	Tyr (Y)	14	15	16	15	8
	Val (V)	28	27	36	25	20
	Total Amino Acid	358	358	520	462	351
	Carbon C	1805	1810	2654	2352	1845
	Hydrogen H	2687	2679	3940	3501	2718
	Nitrogen N	463	459	656	603	454
	Oxygen O	495	497	714	626	478
	Sulfur S	18	15	13	16	13
	Total atoms	5468	5460	7977	7098	5508

Total Amino Acid / RCII	3357
Protein Carbon C / RCII	16869
Protein Hydrogen H / RCII	25798
Protein Nitrogen N / RCII	4338
Protein Oxygen O / RCII	4722
Protein Sulfur S / RCII	115
Total protein atoms / RCII	51842

Stressed PSII includes a D1:2 protein

Total Amino Acid / RCII	3357
Protein Carbon C / RCII	16874
Protein Hydrogen H / RCII	25790
Protein Nitrogen N / RCII	4334
Protein Oxygen O / RCII	4724
Protein Sulfur S / RCII	112
Total protein atoms / RCII	51834

					Reaction Center II		
psbE	***psbF***	***psbH***	***psbI***	***psbJ***	***psbK***	***psbL***	***psbM***
alpha cyt b559	**beta cyt b559**	**PsbH**	**PsbI**	**PsbJ**	**PsbK**	**PsbL**	**PsbM**
FLFVSTGLAYDAFVRWLALHTLGVVMGIFMALFLVLGIFVFGFLSWTEGTLPLWVGPLIDILPIVRTSLYLGLLFVLVPTVFLI							
9089	5093	7547,05	4414	7025	5268	4537,21	3976,66
6,55	12	9,52	5,92	9,82	4,03	5,9	4,14
35,15	41,12	32,46	25,97	44,75	24,18	23,46	15,06
86,95	91,11	133,24	104,87	87,12	143,4	107,87	118,89
0,163	0,396	0,612	0,674	0,206	1,174	0,141	0,906
RCII	RCII	RCII	RCII	RCII	RCII	RCII	RCII
9	5	2	2	6	7	0	1
5	4	3	2	4	1	2	1
0	1	5	0	1	0	6	2
3	0	1	3	3	2	0	1
0	0	0	0	0	0	0	0
2	2	2	0	0	3	1	1
5	0	2	1	1	1	2	2
6	2	9	2	10	2	2	2
1	1	0	0	0	0	0	0
6	2	5	2	2	4	2	2
7	5	14	5	6	10	7	5
3	0	2	2	3	0	0	0
1	2	3	1	2	1	1	2
8	4	3	6	3	5	4	4
5	4	3	2	5	4	2	1
8	1	2	5	5	1	3	4
5	7	3	1	3	1	3	3
1	1	2	0	3	1	0	0
3	1	2	1	2	2	2	0
4	3	5	4	7	2	2	5
82	45	68	39	66	47	39	36
422	237	352	210	324	259	209	182
641	369	562	319	499	390	320	288
105	63	88	47	85	54	52	42
117	58	89	55	86	61	59	53
1	2	3	1	2	1	1	2
1286	729	1094	632	996	765	641	567

psbN PsbN	*psbO* PsbO	*psbP* CyanoP	*psbQ* CyanoQ	*psbT* PsbT	*psbU* PsbU	*psbV* cyt c-550	*psbX* PsbX	*psbY* PsbY	*psbZ* Ycf9
GLGVYTAFG	LVPGGEEAVAVGERLIHGPM	AIATLFFPGMYPTFQNVGLDTE					AIVVIPASAWAGFNIG	SNEDSGR	
4031,55	29319	20177	16657	3428	13958	18409	4250,02	4334	6705,06
3,9	4,56	5,18	8,33	8,25	4,94	4,81	5,71	12	5,82
37,64	33,99	41,79	36,37	29,05	26,67	41,36	7,22	65,45	38,42
105,13	78,24	101,14	90,72	129,35	102,08	99,29	131,5	146,5	161,77
0,362	-0,185	0,022	-0,107	1,087	-0,174	0,058	0,925	0,863	1,347
RCII	RCII	RCII	RCII	RCII	RCII	RCII	RCII	RCII	RCII
5	20	16	24	5	7	17	3	7	6
0	14	16	13	1	9	9	1	4	2
1	8	6	7	0	7	5	1	1	4
5	20	12	7	1	11	13	2	1	1
0	4	2	5	0	0	2	0	0	0
0	7	4	8	0	4	5	2	2	1
1	19	11	9	1	7	7	0	0	1
4	31	13	8	2	11	14	2	3	4
1	1	4	1	0	0	2	0	0	0
1	16	6	6	5	6	8	3	3	4
6	21	22	18	4	16	22	6	8	12
1	11	1	5	2	6	5	1	1	0
1	6	1	4	1	2	4	1	2	2
2	15	7	5	4	6	5	3	1	2
3	13	7	6	2	6	8	2	1	1
2	20	15	6	1	7	11	5	2	5
2	22	13	9	1	3	13	3	0	2
0	0	2	1	0	1	2	0	1	2
1	8	5	3	1	4	6	0	0	2
3	17	21	7	0	12	12	5	3	11
39	273	184	152	31	125	170	40	40	62
182	1289	893	724	167	626	819	195	197	315
281	2025	1417	1178	260	994	1300	319	335	507
43	343	253	214	36	170	218	47	57	75
58	417	274	218	39	187	251	56	48	81
1	10	3	9	1	2	6	1	2	2
565	4084	2840	2343	503	1979	2594	618	639	980

psb28		Gene name	*psaA*	*psaB*	*psaC*	*psaD*
Psb29		Gene product	PsaA	PsaB	PsaC	PsaD
EEGTLVTREVNGKFVN		Protein sequence	MTISPPI	MTEEKL	MSHAVI	MTASALTGC
14067,6		MW (da)	83858	77709	8828	15726
4,46		pI	6,84	6,5	5,15	6,74
		Stability	21,3	23,97	53,44	42,85
		Aliphatic index	94	92,64	72,22	66,22
		GRAVY	0,257	0,241	0,025	-0,434
RCII		Complex	RCI	RCI	RCI	RCI
14		Ala (A)	85	78	6	10
9		Arg (R)	19	16	5	8
4		Asn (N)	29	32	0	6
9		Asp (D)	32	24	6	4
0		Cys (C)	3	3	9	1
6		Gln (Q)	26	24	2	5
13		Glu (E)	16	18	4	12
12		Gly (G)	77	72	6	15
0		His (H)	44	39	1	2
4		Ile (I)	51	45	4	8
6		Leu (L)	75	72	5	10
4		Lys (K)	24	17	3	8
5		Met (M)	24	16	3	4
8		Phe (F)	50	50	1	9
4		Pro (P)	31	27	4	8
9		Ser (S)	50	37	6	12
7		Thr (T)	37	37	6	11
1		Trp (W)	27	29	1	1
3		Tyr (Y)	17	26	3	4
10		Val (V)	50	40	6	5
128		Total Amino Acid	767	702	81	143
611		Carbon C	3873	3632	373	697
948		Hydrogen H	5802	5320	598	1087
170		Nitrogen N	1018	930	104	191
202		Oxygen O	1023	943	119	214
5		Sulfur S	27	19	12	5
1936		Total atoms	11743	10844	1206	2194

Total Amino Acid / RCI	2288
Protein Carbon C / RCI	11475
Protein Hydrogen H / RCI	17311
Protein Nitrogen N / RCI	2975
Protein Oxygen O / RCI	3104
Protein Sulfur S / RCI	90
Total protein atoms / RCI	34955

	Reaction Center I					
psaE	***psaF***	***psaI***	***psaJ***	***psaK***	***psaL***	***psaM***
PsaE	**PsaF**	**PsaI**	**PsaJ**	**PsaK**	**PsaL**	**PsaM**
MAISRGDKV	MRRLFALAL	MTGEFVAAV	MKKFLTTAP	MTSHLLAVA	MTVTPVADF	MVGRYESVMVSSITQTEI
7593,5	17203,9	3996,81	4494,42	8763	16792	4525
6,15	7,71	3,57	8,37	6,7	4,99	7,98
17,16	25,43	48,1	33,29	25,43	31,09	12,85
76,23	90,38	112,89	105,13	119,3	8801	134,52
-0,384	0,154	1,297	0,762	0,839	0,48	1,119
RCI	RCI	RCI	RCI	RCI	RCI	RCI
5	23	6	4	7	22	6
5	9	0	1	0	4	3
6	0	1	1	2	7	0
3	7	1	1	0	6	0
0	3	0	0	1	3	1
1	5	0	0	2	1	1
5	9	2	1	3	2	2
7	14	3	2	13	21	2
0	2	0	1	2	1	1
6	7	2	3	5	7	3
1	18	3	5	14	16	4
3	8	0	2	3	2	0
1	4	4	2	2	4	2
3	9	3	5	5	10	1
3	7	3	3	4	14	0
6	11	1	0	6	9	4
3	8	2	4	6	14	2
1	3	1	2	1	4	0
3	4	0	0	2	5	2
7	8	6	2	7	11	8
69	159	38	39	85	163	42
335	778	186	219	408	771	203
523	1220	288	327	643	1167	336
95	206	40	49	97	191	54
105	220	49	49	110	216	56
1	7	4	2	3	7	3
1059	2431	567	646	1261	2352	652

	OCP
Gene name	**ocp**
Gene product	**Ocp**
Protein sequence	MFTIDKAAQIFPDTRTADAVPAITARYKLLSAEDQLALIWFAYLEMGI
MW (da)	34895
pI	4,6
Stability	25,31
Aliphatic index	95,72
GRAVY	0,036
Complex	OCP
Ala (A)	30
Arg (R)	11
Asn (N)	13
Asp (D)	22
Cys (C)	2
Gln (Q)	16
Glu (E)	17
Gly (G)	26
His (H)	0
Ile (I)	22
Leu (L)	32
Lys (K)	16
Met (M)	9
Phe (F)	18
Pro (P)	19
Ser (S)	15
Thr (T)	15
Trp (W)	5
Tyr (Y)	8
Val (V)	22
Total Amino Acid	318
Carbon C	1583
Hydrogen H	2469
Nitrogen N	401
Oxygen O	464
Sulfur S	11
Total atoms	4928

RTITVAAPGAARMAIAQPTLDEITGMGFSEQSRVMCDLAGKVDAPISTRYAFWSINVKLGFWYELGELMNQGK


CVAPIPEGYKLSSNANAVLESVKKVEQGQQISILRNFVVDMGFDPDNDDSAIVSEPIVEPTPAEARVKVFIPGVLN

NQTILDYMELLNSNDFDGLIKLFLSDGALQPPFQRPIVGTDAILKFFKRDCQNLKLLPQGGYGEPTDGGFNQIK

VTGQVQTPWFGGEVGMNVAWRFLLDENDKIYFVAIDLLASPAELLKLGGS

	Exp. Data	zmol hexamer / cell				zmol/cell
	Growth T°C	Beta-PE	R-PC	AP	PsbD (D2)	PsaC
MVIR-18-1	9	84,0	21,0	12,6	2,3	5,1
	13	100,6	25,1	15,1	2,8	10,1
	16	101,4	22,5	13,7	2,9	11,4
	18	112,9	22,6	13,5	4,2	13,2
	22	169,9	34,0	20,4	5,0	17,3
	25	204,0	40,8	24,5	5,5	25,0

	Amino acid allocation	2458	2510	2946	7914	3357
	Growth T°C	PE	PC	AP	PBS	RCII
MVIR-18-1	9	2,1E+05	5,3E+04	3,7E+04	3,0E+05	
	13	2,5E+05	6,3E+04	4,4E+04	3,5E+05	
	16	2,5E+05	5,7E+04	4,0E+04	3,5E+05	
	18	2,8E+05	5,7E+04	4,0E+04	3,7E+05	1,4E+04
	22	4,2E+05	8,5E+04	6,0E+04	5,6E+05	1,7E+04
	25	5,0E+05	1,0E+05	7,2E+04	6,8E+05	1,9E+04

	Carbon allocation	12130	12348	14852	39330	16869
	Growth T°C	PE	PC	AP	PBS	RCII
MVIR-18-1	9	1,0E+06	2,6E+05	1,9E+05	1,5E+06	
	13	1,2E+06	3,1E+05	2,2E+05	1,8E+06	
	16	1,2E+06	2,8E+05	2,0E+05	1,7E+06	
	18	1,4E+06	2,8E+05	2,0E+05	1,8E+06	6,0E+04
	22	2,1E+06	4,2E+05	3,0E+05	2,8E+06	7,0E+04
	25	2,5E+06	5,0E+05	3,6E+05	3,3E+06	7,8E+04

	Nitrogen allocation	3312	3347	3921	10580	4338
	Growth T°C	PE	PC	AP	PBS	RCII
MVIR-18-1	9	2,8E+05	7,0E+04	4,9E+04	4,0E+05	
	13	3,3E+05	8,4E+04	5,9E+04	4,8E+05	
	16	3,4E+05	7,5E+04	5,4E+04	4,6E+05	
	18	3,7E+05	7,6E+04	5,3E+04	5,0E+05	1,8E+04
	22	5,6E+05	1,1E+05	8,0E+04	7,6E+05	2,2E+04
	25	6,8E+05	1,4E+05	9,6E+04	9,1E+05	2,4E+04

	Sulfur allocation	113	102	128	344	115
	Growth T°C	PE	PC	AP	PBS	RCII
MVIR-18-1	9	9,5E+03	2,1E+03	1,6E+03	1,3E+04	
	13	1,1E+04	2,6E+03	1,9E+03	1,6E+04	
	16	1,1E+04	2,3E+03	1,8E+03	1,6E+04	
	18	1,3E+04	2,3E+03	1,7E+03	1,7E+04	4,9E+02
	22	1,9E+04	3,5E+03	2,6E+03	2,5E+04	5,7E+02
	25	2,3E+04	4,2E+03	3,1E+03	3,0E+04	6,3E+02

	Iron allocation	1	12	zmol/cell
	Growth T°C	PSII	PSI	TOTAL
MVIR-18-1	9	2,3	61,3	63,6
	13	2,8	120,9	123,711
	16	2,9	137,0	139,853
	18	4,2	158,9	163,112

	22	5,0	208,2	213,14
	25	5,5	300,4	305,878

	Molecular Weight (g/mol)					
	893,51	536,87	568,88	552,85	566,87	
	fg/cell					
OCP	**Chl a**	**β-Car**	**Zea**	**β-Crypto**	**3'-OH Ech**	**Predicted Phaeo a**
42,9	0,88	0,12	1,35	0,02	0,02	5
19,5	0,97	0,12	1,10	0,01	0,01	6
19,8	1,16	0,18	1,08	0,02	0,01	6
13,8	1,18	0,18	1,06	0,02	0,01	8
8,1	1,51	0,21	1,08	0,02	0,00	10
8,7	1,73	0,23	1,27	0,03	0,00	11

3357	2288	318	0	0	0	0
Stress RCII	**RCI**	**OCP**	**Chl a**	**β-Car**	**Zea**	**β-Crypto**
7,7E+03	1,2E+04	1,4E+04	0	0	0	0
9,6E+03	2,3E+04	6,2E+03	0	0	0	0
9,7E+03	2,6E+04	6,3E+03	0	0	0	0
	3,0E+04	4,4E+03	0	0	0	0
	4,0E+04	2,6E+03	0	0	0	0
	5,7E+04	2,8E+03	0	0	0	0

16874	11475	1583	55	40	40	40
Stress RCII	**RCI**	**OCP**	**Chl a**	**β-Car**	**Zea**	**β-Crypto**
3,9E+04	5,9E+04	6,8E+04	5,4E+04	9,0E+03	9,5E+04	1,1E+03
4,8E+04	1,2E+05	3,1E+04	6,0E+04	9,1E+03	7,7E+04	9,2E+02
4,9E+04	1,3E+05	3,1E+04	7,1E+04	1,3E+04	7,6E+04	1,5E+03
	1,5E+05	2,2E+04	7,3E+04	1,3E+04	7,4E+04	1,3E+03
	2,0E+05	1,3E+04	9,3E+04	1,6E+04	7,6E+04	1,6E+03
	2,9E+05	1,4E+04	1,1E+05	1,7E+04	8,9E+04	2,0E+03

4334	2975	401	4	0	0	0
Stress RCII	**RCI**	**OCP**	**Chl a**	**β-Car**	**Zea**	**β-Crypto**
1,0E+04	1,5E+04	1,7E+04	3,9E+03	0	0	0
1,2E+04	3,0E+04	7,8E+03	4,3E+03	0	0	0
1,8E+04	3,4E+04	7,9E+03	5,2E+03	0	0	0
	3,9E+04	5,5E+03	5,3E+03	0	0	0
	5,2E+04	3,2E+03	6,8E+03	0	0	0
	7,4E+04	3,5E+03	7,8E+03	0	0	0

112	90	11	0	0	0	0
Stress RCII	**RCI**	**OCP**	**Chl a**	**β-Car**	**Zea**	**β-Crypto**
2,6E+02	4,6E+02	4,7E+02	0	0	0	0
3,2E+02	9,1E+02	2,1E+02	0	0	0	0
3,3E+02	1,0E+03	2,2E+02	0	0	0	0
	1,2E+03	1,5E+02	0	0	0	0
	1,6E+03	8,9E+01	0	0	0	0
	2,3E+03	9,6E+01	0	0	0	0

zmol/cell				
Chl a	**β-Car**	**Zea**	**β-Crypto**	**3'-OH Ech**
984	225	2378	27	43
1086	228	1928	23	20
1294	330	1905	38	20
1322	328	1862	34	14
1689	396	1890	39	8
1940	426	2225	50	9

0	0	Amino acid	Amino acid
3'-OH Ech	**Phaeophytin a**	**TOTAL (zmol/cell)**	**TOTAL (fmol/cell)**
0	0	6,3E+05	**0,63**
0	0	7,5E+05	**0,75**
0	0	7,3E+05	**0,73**
0	0	8,0E+05	**0,80**
0	0	1,2E+06	**1,18**
0	0	1,4E+06	**1,43**

40	55	Carbon	Carbon	Carbon
3'-OH Ech	**Phaeophytin a**	**TOTAL (zmol/cell)**	**TOTAL (fmol/cell)**	**TOTAL (fg/cell)**
1,7E+03	2,5E+02	3,3E+06	**3,3**	**39,1**
7,8E+02	3,1E+02	3,9E+06	**3,9**	**46,2**
7,9E+02	3,2E+02	3,8E+06	**3,8**	**45,6**
5,5E+02	4,6E+02	4,1E+06	**4,1**	**49,1**
3,2E+02	5,5E+02	6,0E+06	**6,0**	**72,4**
3,5E+02	6,1E+02	7,3E+06	**7,3**	**87,4**

0	4	Nitrogen	Nitrogen	Nitrogen
3'-OH Ech	**Phaeophytin a**	**TOTAL (zmol/cell)**	**TOTAL (fmol/cell)**	**TOTAL (fg/cell)**
0	1,8E+01	8,4E+05	**0,84**	**11,8**
0	2,3E+01	1,0E+06	**1,01**	**14,1**
0	2,3E+01	1,0E+06	**1,00**	**13,9**
0	3,4E+01	1,1E+06	**1,07**	**15,0**
0	4,0E+01	1,6E+06	**1,60**	**22,3**
0	4,4E+01	1,9E+06	**1,93**	**27,0**

0	0	Sulfur	Sulfur	Sulfur
3'-OH Ech	**Phaeophytin a**	**TOTAL (zmol/cell)**	**TOTAL (fmol/cell)**	**TOTAL (fg/cell)**
0	0	2,8E+04	**0,03**	**0,9**
0	0	3,3E+04	**0,03**	**1,1**
0	0	3,3E+04	**0,03**	**1,0**
0	0	3,6E+04	**0,04**	**1,1**
0	0	5,3E+04	**0,05**	**1,7**
0	0	6,4E+04	**0,06**	**2,0**

	Exp. Data	zmol hexamer /
	Growth T°C	Beta-PE	R-PC
M16.1	17	43,9	11,0
	18	43,7	10,9
	22	90,0	20,0
	25	141,1	28,2
	28	203,6	40,7
	31	412,0	82,4

	Amino acid allocation	2426	2512
	Growth T°C	PE	PC
M16.1	17	1,1E+05	2,8E+04
	18	1,1E+05	2,7E+04
	22	2,2E+05	5,0E+04
	25	3,4E+05	7,1E+04
	28	4,9E+05	1,0E+05
	31	1,0E+06	2,1E+05

	Carbon allocation	12244	12323
	Growth T°C	PE	PC
M16.1	17	5,4E+05	1,4E+05
	18	5,3E+05	1,3E+05
	22	1,1E+06	2,5E+05
	25	1,7E+06	3,5E+05
	28	2,5E+06	5,0E+05
	31	5,0E+06	1,0E+06

C:N ratio
3,32
3,28
3,27
3,27
3,24
3,24

	Nitrogen allocation	3339	3345
	Growth T°C	PE	PC
M16.1	17	1,5E+05	3,7E+04
	18	1,5E+05	3,7E+04
	22	3,0E+05	6,7E+04
	25	4,7E+05	9,4E+04
	28	6,8E+05	1,4E+05
	31	1,4E+06	2,8E+05

	Sulfur allocation	114	104
	Growth T°C	PE	PC
M16.1	17	5,0E+03	1,1E+03
	18	5,0E+03	1,1E+03
	22	1,0E+04	2,1E+03
	25	1,6E+04	2,9E+03
	28	2,3E+04	4,2E+03
	31	4,7E+04	8,6E+03

	Iron allocation	1	12
	Growth T°C	PSII	PSI
M16.1	17	2,2	64,1
	18	1,5	75,1
	22	2,0	93,0
	25	2,8	113,4

	28	4,7	222,4
	31	9,5	344,1

				Molecular Weight (g/mol)			
				893,51	536,87	568,88	552,85
cell	zmol/cell			fg/cell			
AP	PsbD (D2)	PsaC	OCP	Chl a	β-Car	Zea	Beta-Crypto
6,6	2,2	5,3	3,2	1,33	0,08	1,01	0,01
6,6	1,5	6,3	3,6	0,99	0,08	1,06	0,01
12,1	2,0	7,8	2,5	1,09	0,12	1,03	0,01
16,9	2,8	9,5	2,0	1,34	0,16	1,12	0,01
24,4	4,7	18,5	2,3	2,43	0,30	1,65	0,02
49,4	9,5	28,7	4,1	3,39	0,43	2,23	0,04

2946	7884	3352	3353	2311	318	0	0
AP	PBS	RCII	Stress RCII	RCI	OCP	Chl a	β-Car
1,9E+04	1,5E+05		7,5E+03	1,2E+04	1,0E+03	0	0
1,9E+04	1,5E+05		5,0E+03	1,4E+04	1,2E+03	0	0
3,6E+04	3,0E+05		6,6E+03	1,8E+04	8,0E+02	0	0
5,0E+04	4,6E+05	9,3E+03		2,2E+04	6,5E+02	0	0
7,2E+04	6,7E+05	1,6E+04		4,3E+04	7,3E+02	0	0
1,5E+05	1,4E+06	3,2E+04		6,6E+04	1,3E+03	0	0

14852	39419	16669	16675	11605	1621	55	40
AP	PBS	RCII	Stress RCII	RCI	OCP	Chl a	β-Car
9,8E+04	7,7E+05		3,7E+04	6,2E+04	5,1E+03	8,2E+04	5,8E+03
9,7E+04	7,7E+05		2,5E+04	7,3E+04	5,9E+03	6,1E+04	6,1E+03
1,8E+05	1,5E+06		3,3E+04	9,0E+04	4,1E+03	6,7E+04	9,0E+03
2,5E+05	2,3E+06	4,6E+04		1,1E+05	3,3E+03	8,2E+04	1,2E+04
3,6E+05	3,4E+06	7,8E+04		2,2E+05	3,7E+03	1,5E+05	2,2E+04
7,3E+05	6,8E+06	1,6E+05		3,3E+05	6,6E+03	2,1E+05	3,2E+04

3921	10605	4321	4316	3036	409	4	0
AP	PBS	RCII	Stress RCII	RCI	OCP	Chl a	β-Car
2,6E+04	2,1E+05		9,6E+03	1,6E+04	1,3E+03	6,0E+03	0
2,6E+04	2,1E+05		6,5E+03	1,9E+04	1,5E+03	4,4E+03	0
4,8E+04	4,2E+05		8,5E+03	2,4E+04	1,0E+03	4,9E+03	0
6,6E+04	6,3E+05	1,2E+04		2,9E+04	8,4E+02	6,0E+03	0
9,6E+04	9,1E+05	2,0E+04		5,6E+04	9,4E+02	1,1E+04	0
1,9E+05	1,8E+06	4,1E+04		8,7E+04	1,7E+03	1,5E+04	0

128	347	117	114	86	13	0	0
AP	PBS	RCII	Stress RCII	RCI	OCP	Chl a	β-Car
8,5E+02	7,0E+03		2,5E+02	4,6E+02	4,1E+01	0	0
8,4E+02	7,0E+03		1,7E+02	5,4E+02	4,7E+01	0	0
1,6E+03	1,4E+04		2,3E+02	6,7E+02	3,3E+01	0	0
2,2E+03	2,1E+04	3,2E+02		8,1E+02	2,7E+01	0	0
3,1E+03	3,1E+04	5,4E+02		1,6E+03	3,0E+01	0	0
6,3E+03	6,2E+04	1,1E+03		2,5E+03	5,3E+01	0	0

zmol/cell
TOTAL
66,3
76,6
95,0
116,2

227,1
353,7

566,87

			zmol/cell
3'-OH Ech	**Predicted Phaeo a**	**Chl a**	**β-Car**
0,002	4	1494	144
0,002	3	1108	152
0,001	4	1225	224
0,001	6	1497	298
0,001	9	2714	561
0,002	19	3793	809

0	0	0	0
Zea	**Beta-Crypto**	**3'-OH Ech**	**Phaeophytin a**
0	0	0	0
0	0	0	0
0	0	0	0
0	0	0	0
0	0	0	0
0	0	0	0

40	40	40	55
Zea	**Beta-Crypto**	**3'-OH Ech**	**Phaeophytin a**
7,1E+04	4,0E+02	1,3E+02	2,5E+02
7,4E+04	5,1E+02	1,4E+02	1,7E+02
7,2E+04	7,1E+02	1,0E+02	2,2E+02
7,9E+04	9,1E+02	8,2E+01	3,0E+02
1,2E+05	1,8E+03	9,2E+01	5,1E+02
1,6E+05	2,7E+03	1,6E+02	1,0E+03

0	0	0	4
Zea	**Beta-Crypto**	**3'-OH Ech**	**Phaeophytin a**
0	0	0	1,8E+01
0	0	0	1,2E+01
0	0	0	1,6E+01
0	0	0	2,2E+01
0	0	0	3,7E+01
0	0	0	7,6E+01

0	0	0	0
Zea	**Beta-Crypto**	**3'-OH Ech**	**Phaeophytin a**
0	0	0	0
0	0	0	0
0	0	0	0
0	0	0	0
0	0	0	0
0	0	0	0

Zea	Beta-Crypto	3'-OH Ech
1772	10	3
1858	13	4
1806	18	3
1966	23	2
2909	45	2
3922	69	4

Amino acid	Amino acid
TOTAL (zmol/cell)	TOTAL (fmol/cell)
3,3E+05	**0,33**
3,3E+05	**0,33**
6,3E+05	**0,63**
9,6E+05	**0,96**
1,4E+06	**1,40**
2,8E+06	**2,80**

Carbon	Carbon	Carbon
TOTAL (zmol/cell)	TOTAL (fmol/cell)	TOTAL (fg/cell)
1,8E+06	**1,8**	**21,7**
1,8E+06	**1,8**	**21,4**
3,3E+06	**3,3**	**40,0**
5,0E+06	**5,0**	**59,9**
7,3E+06	**7,3**	**87,6**
1,4E+07	**14,5**	**173,8**

Nitrogen	Nitrogen	Nitrogen	C:N ratio
TOTAL (zmol/cell)	TOTAL (fmol/cell)	TOTAL (fg/cell)	
4,5E+05	**0,45**	**6,3**	**3,43**
4,5E+05	**0,45**	**6,3**	**3,41**
8,7E+05	**0,87**	**12,2**	**3,29**
1,3E+06	**1,31**	**18,4**	**3,26**
1,9E+06	**1,91**	**26,8**	**3,27**
3,8E+06	**3,84**	**53,7**	**3,24**

Sulfur	Sulfur	Sulfur
TOTAL (zmol/cell)	TOTAL (fmol/cell)	TOTAL (fg/cell)
1,5E+04	**0,01**	**0,5**
1,5E+04	**0,01**	**0,5**
2,9E+04	**0,03**	**0,9**
4,4E+04	**0,04**	**1,4**
6,3E+04	**0,06**	**2,0**
1,3E+05	**0,13**	**4,1**

Biovolume transformed data

	Growth Temp	Biovolume	zmol hexamer / µm^3			zmol / µm^3			
	°C	(µm^3/cell)	Beta-PE	R-PC	AP	PsbD (D2)	PsaC	OCP	Chl a
MVIR-18-1	**9**	0,59	141	35,3	21,2	3,9	8,6	72,2	1,5
	13	0,58	173	43,3	26,0	4,9	17,4	33,7	1,7
	16	0,53	192	42,7	25,9	5,5	21,6	37,5	2,2
	18	0,63	180	36,0	21,6	6,7	21,1	22,0	1,9
	22	0,59	290	58,0	34,8	8,5	29,6	13,8	2,6
	25	0,78	262	52,4	31,4	7,1	32,1	11,2	2,2

	Growth Temp	Biovolume	zmol hexamer / µm^3			zmol / µm^3			
	°C	(µm^3/cell)	Beta-PE	R-PC	AP	PsbD (D2)	PsaC	OCP	Chl a
M16.1	**16,5**	0,35	125	31,2	18,7	6,3	15,2	9,0	3,8
	18	0,37	117	29,2	17,5	4,0	16,7	9,7	2,6
	22	0,30	301	66,9	40,6	6,6	25,9	8,4	3,7
	28	0,50	407	81,4	48,8	9,3	37,0	4,6	4,8
	31	0,67	619	123,8	74,3	14,3	43,1	6,1	5,1

fg / µm^3				fmol / µm^3	fg / µm^3			zmol / µm^3
β-Car	**Zea**	**β-Crypto**	**3'-OH Ech**	**AA**	**C**	**N**	**S**	**Fe**
0,2	2,3	0,025	0,041	1,1	66	19,8	1,5	107
0,2	1,9	0,022	0,019	1,3	80	24,3	1,8	213
0,3	2,1	0,040	0,021	1,4	86	26,4	2,0	265
0,3	1,7	0,030	0,012	1,3	78	24,0	1,8	260
0,4	1,8	0,037	0,008	2,0	124	38,2	2,9	364
0,3	1,6	0,036	0,006	1,8	112	34,6	2,6	393

fg / µm^3				fmol / µm^3	fg / µm^3			zmol / µm^3
β-Car	**Zea**	**β-Crypto**	**3'-OH Ech**	**AA**	**C**	**N**	**S**	**Fe**
0,2	2,9	0,016	0,005	0,9	61	17,9	1,3	188
0,2	2,8	0,019	0,005	0,9	57	16,8	1,3	205
0,4	3,4	0,033	0,005	2,1	134	40,7	3,1	318
0,6	3,3	0,049	0,003	2,8	175	53,5	4,1	454
0,7	3,4	0,057	0,003	4,2	261	80,7	6,1	531

Marine *Synechococcus* Picocyanobacteria: Light Utilization Across Latitudes

Christophe Six, Morgane Ratin, Dominique Marie & Erwan Corre.

Corresponding author: C. Six, six@sb-roscoff.fr

SUPPLEMENTARY INFORMATION

Table of content:

SUPPLEMENTARY MATERIAL

Section 1: Thermal photophysiology of marine *Synechococcus*

Table S1: Information regarding the marine *Synechococcus* strains used in this study. The phylogenetic position has been shown in several studies including (1–4). The pigment types were defined in (5, 6). **PEB**, phycoerythrobilin; **PUB**, phycourobilin; **CA**, chromatic adapter.

Strain name	RCC #	Isolation latitude	Isolation longitude	Isolation site	Phylogenetic position	Phycobilisome pigment type	Ecotype
M16.1	791	+27.70	-91.30	Gulf of Mexico	Clade IIa	3a (PEB-rich)	Tropical
RS9907	2382	+29.47	+34.92	Gulf of Aqaba	Clade IIa	3a (PEB-rich)	Tropical
A15-44	2527	+21.68	+17.83	Sahara coast	Clade IIa	2 (PEB)	Tropical
WH7803	752	+33.75	-67.50	Sargasso Sea	Clade V	3a (PEB-rich)	Coastal tropical
RS9915	2553	+ 29.47	+34.92	Gulf of Aqaba	Clade IIIa	3d (CA)	Warm-temperate
WH8102	539	+22.48	-65.60	Caribbean Sea	Clade IIIa	3c (PUB-rich)	Warm-temperate
BOUM118	2421	+33.63	+32.63	East Med Sea	Clade IIIa	3c (PUB-rich)	Warm-temperate
BL107	515	+41.72	+3.55	Balearic Sea	Clade IVa	3d (CA)	Cold temperate
MVIR-16-1	2570	+60.32	-3.48	North Sea	Clade IVa	3d (CA)	Cold temperate
MVIR-18-1	2385	+61.00	+1.98	Norway Sea	Clade Ib	3a (PEB-rich)	Coastal subpolar
SYN20	2035	+60.27	+5.20	Norway Sea	Clade Ib	3a (PEB-rich)	Coastal subpolar
WH8016	2535	+41.52	-70.67	Buzzards Bay	Clade Ib	3a (PEB-rich)	Coastal subpolar

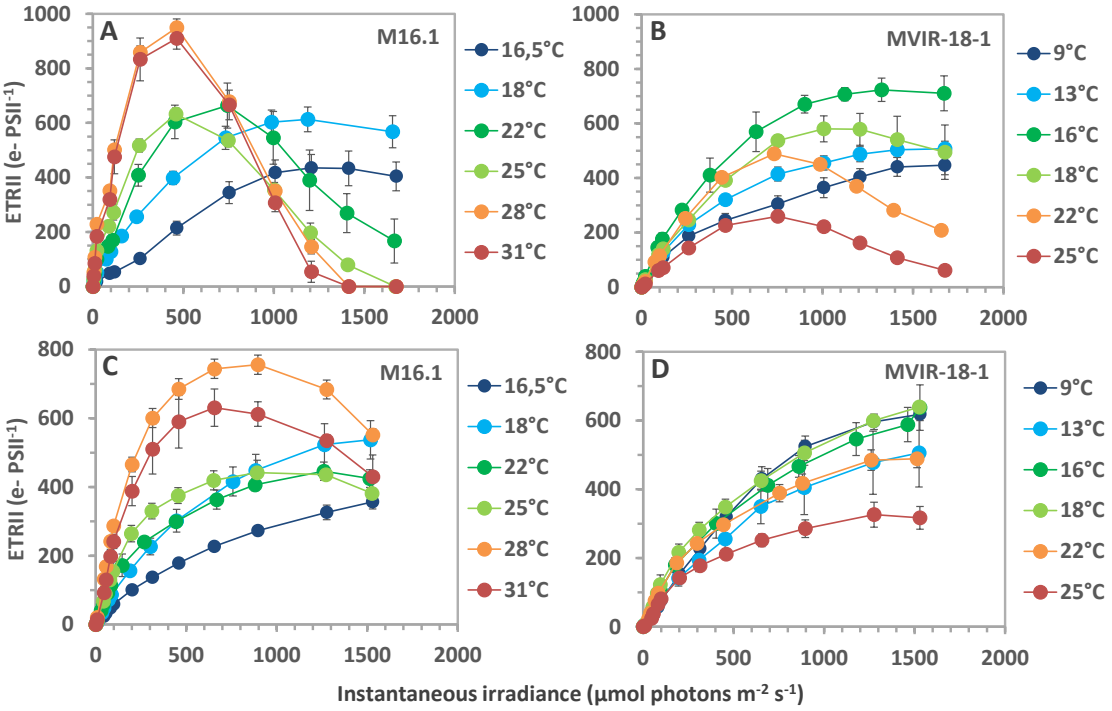

Figure S1: Photosystem II electron transport versus irradiance (photosynthesis / Energy; P/E) curves recorded by pulse amplitude modulation fluorometry. The initial slope α and the saturation irradiance E_K were retrieved by fitting the Platt model (7). Curves recorded at 540 nm for *Synechococcus* spp. M16.1 (**A**) and MVIR-18-1 (**B**) at different growth temperatures. Curves recorded at 480 nm for *Synechococcus* spp. M16.1 (**C**) and MVIR-18-1 (**D**) at different growth temperatures.

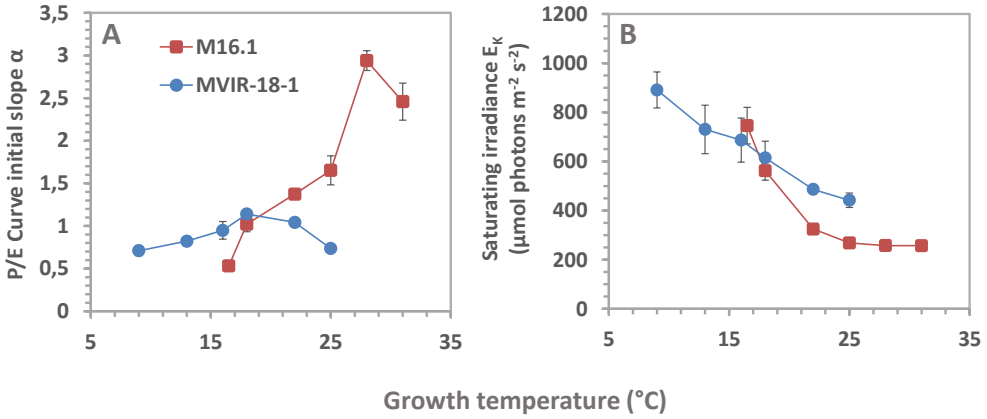

Figure S2: Variations of the initial curve slope α (**A**) and the saturation irradiance (**B**) using 480 nm light, in Synechococcus spp. M16.1 (red) and MVIR-18-1 (blue).

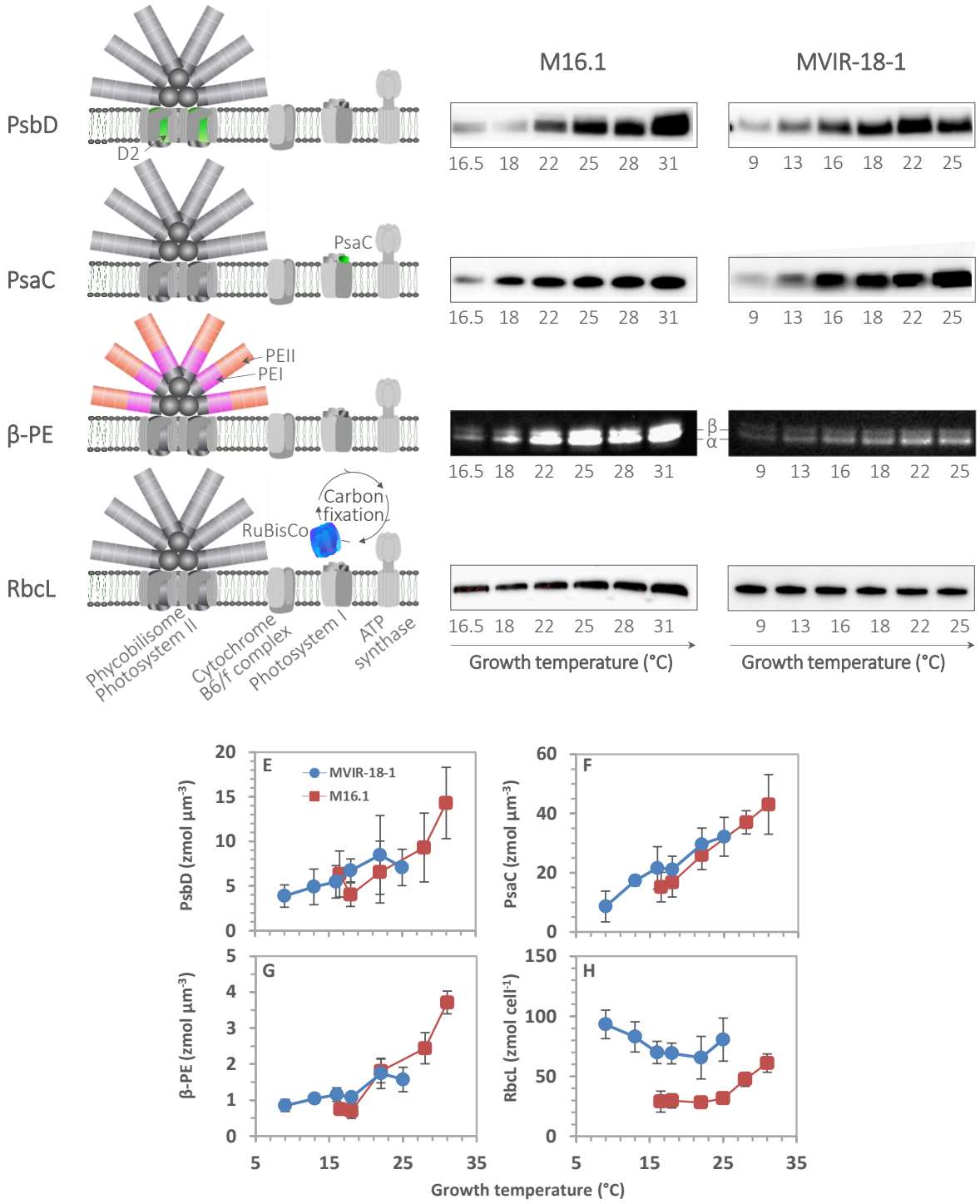

Figure S3: In-gel fluorescence photo (**A**), immunoblots (**B**, **C**, **D**) and quantified variations of the proteins targeted to represent the major photosynthetic complexes in *Synechococcus* spp. M16.1 and MVIR-18-1, function of growth temperature. **A**: Both phycoerythrins I and II could be quantified by fluorescence using their β-PE subunits CpeB and MpeB, respectively, which have the same optical properties in the *Synechococcus* pigment type 3a (5, 8). **B**: Reaction centers II were quantified using the major core protein PsbD (D2). **C**: Reaction centers I were quantified using the small Fe-S binding protein PsaC. **D**: The Ribulose 1,5-bis phosphate Carboxylase Oxygenase (RuBisCO), catalyzing carbon fixation in the Calvin-Benson cycle, was quantified using its large subunit RbcL. Simplified diagrams illustrate the location of these proteins in the different protein complexes. **E**: Phycoerythrin β-subunits variations expressed in zmol per µm^3 cell. **F**: PsbD variations expressed in zmol per µm^3 cell. **G**: PsaC variations expressed in zmol per µm^3 cell. **H**: RbcL variations expressed in zmol per cell.

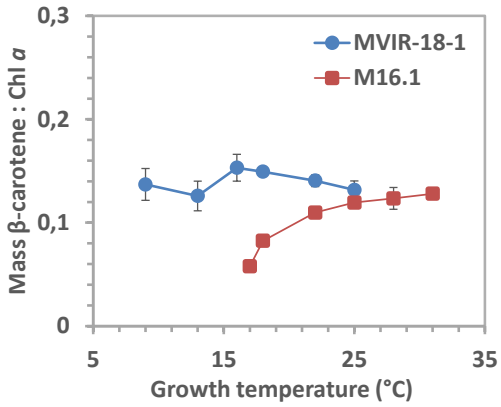

Figure S4: Variations in the mass ratio β-carotene to chlorophyll a in *Synnechococcus* spp. MA6.1 (red) and MVIR-18-1 (blue) grown over their thermal *preferendum*, as measured by high pressure liquid chromatography. The cultures were grown under 80 µmol photons m^{-2} s^{-1} white light.

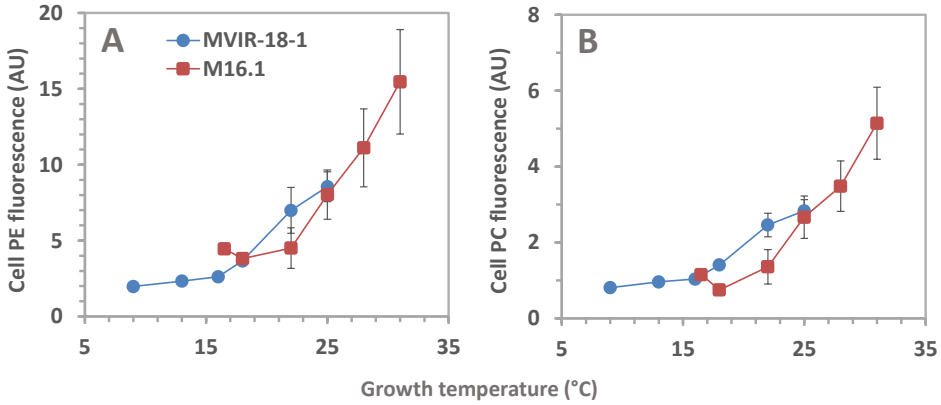

Figure S5: Variations of the cellular phycoerythrin (emission at 565-570 nm; **A**) and phycocyanin (emission at 651 nm; **B**) fluorescences, as measured by cell-normalized spectrofluorometry upon excitation at 530 nm.

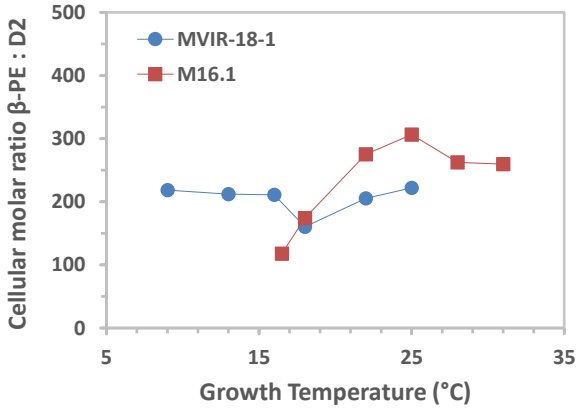

Figure S6: Variations of the cellular molar ratio of β-phycoerythrin (subunits CpeB and MpeB) to PsbD (core protein D2). This ratio is related to the phycobilisome to photosystem II molar ratio in the cells. Note that the values cited in the article are expressed in phycoerythrin hexamers per PsbD proteins.

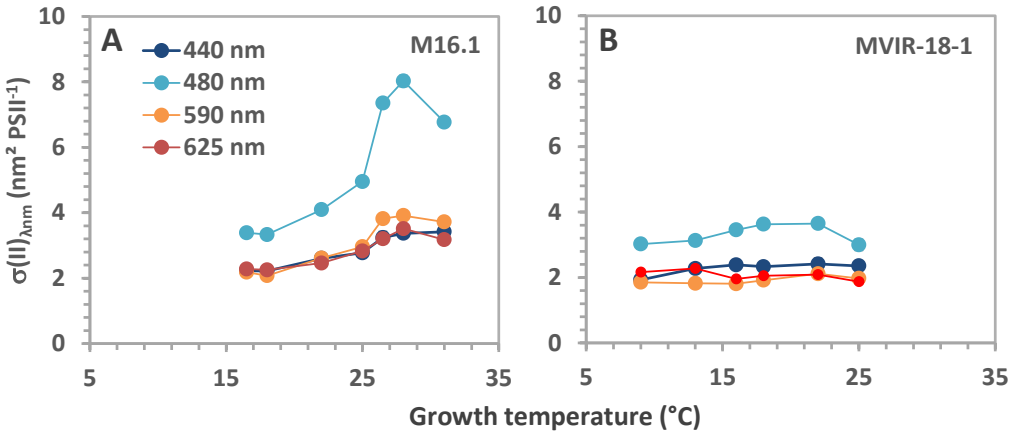

Figure S7: Variations of the photosystem II absorption cross-section at four different wavelengths as measured by recording O-I fast kinetics by pulse amplitude modulation fluorometry, in *Synechococcus* spp. M16.1 (**A**) and MVIR 18-1 (**B**).

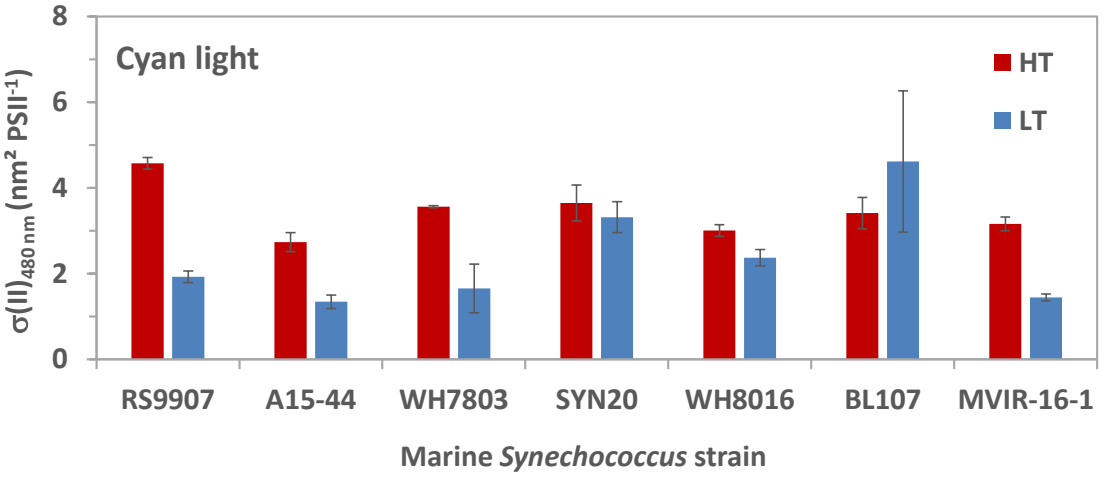

Figure S8: Variations of the photosystem II absorption cross-section at 480 nm in different temperature ecotypes of marine *Synechococcus* grown near their growth thermal limits. These results depend much of the phycourobilin content of the strains, which differ according to the pigment type. Warm adapted strains: RS9907 and A15-44 (Clade II), WH7803 (Clade V); Cold-adapted strains: SYN20 and WH8016 (Clade I), BL107 and MVIR-16-1 (Clade IV).

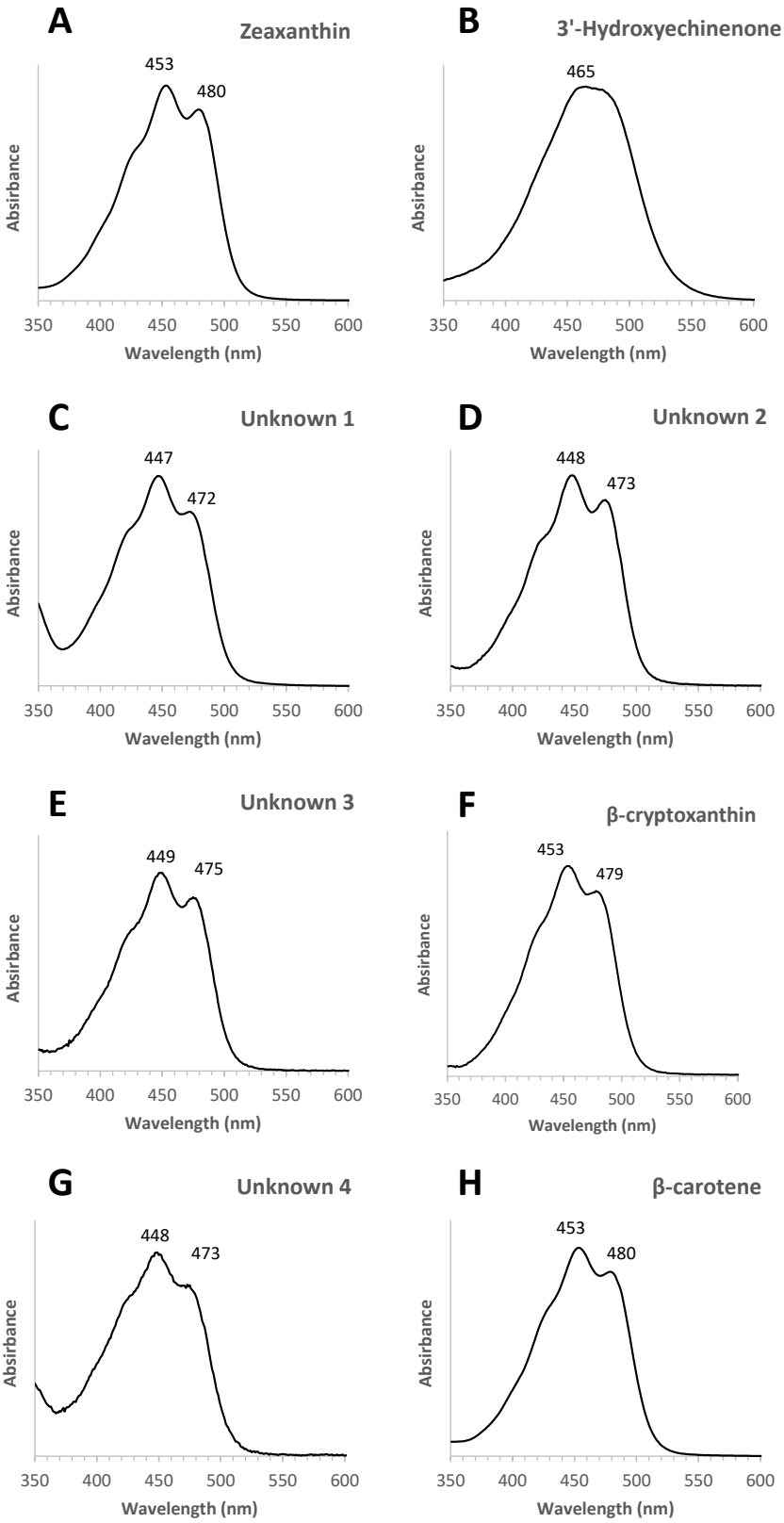

Figure S9: Absorbance spectra of the carotenoids detected in the marine *Synechococcus* strains MVIR-18-1 and M16.1, as measured by a photodiode array at their chromatographic retention time (Please see Fig. S11). Numbers indicate the wavelengths at which absorbance is maximal. Some of the unknown xanthophylls are probably zeaxanthin derivatives.

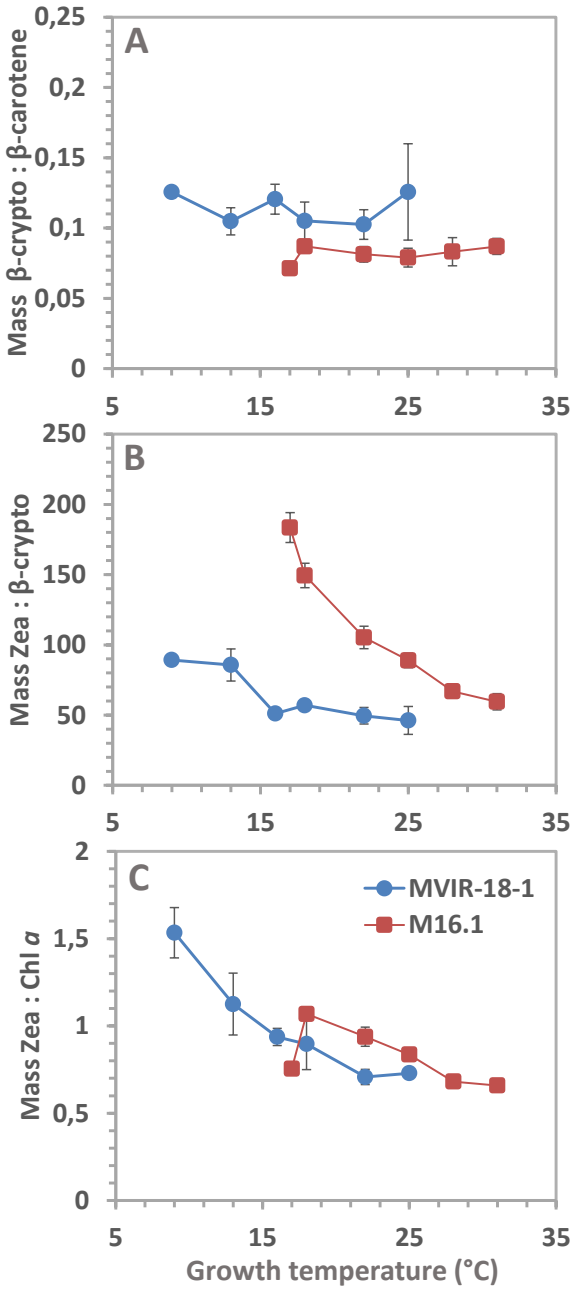

Figure S10: Variations of cellular mass pigment ratios of *Synechococcus* spp. M16.1 (red) and MVIR-18-1 (blue) grown over their thermal preferendum, as measured by high pressure liquid chromatography.

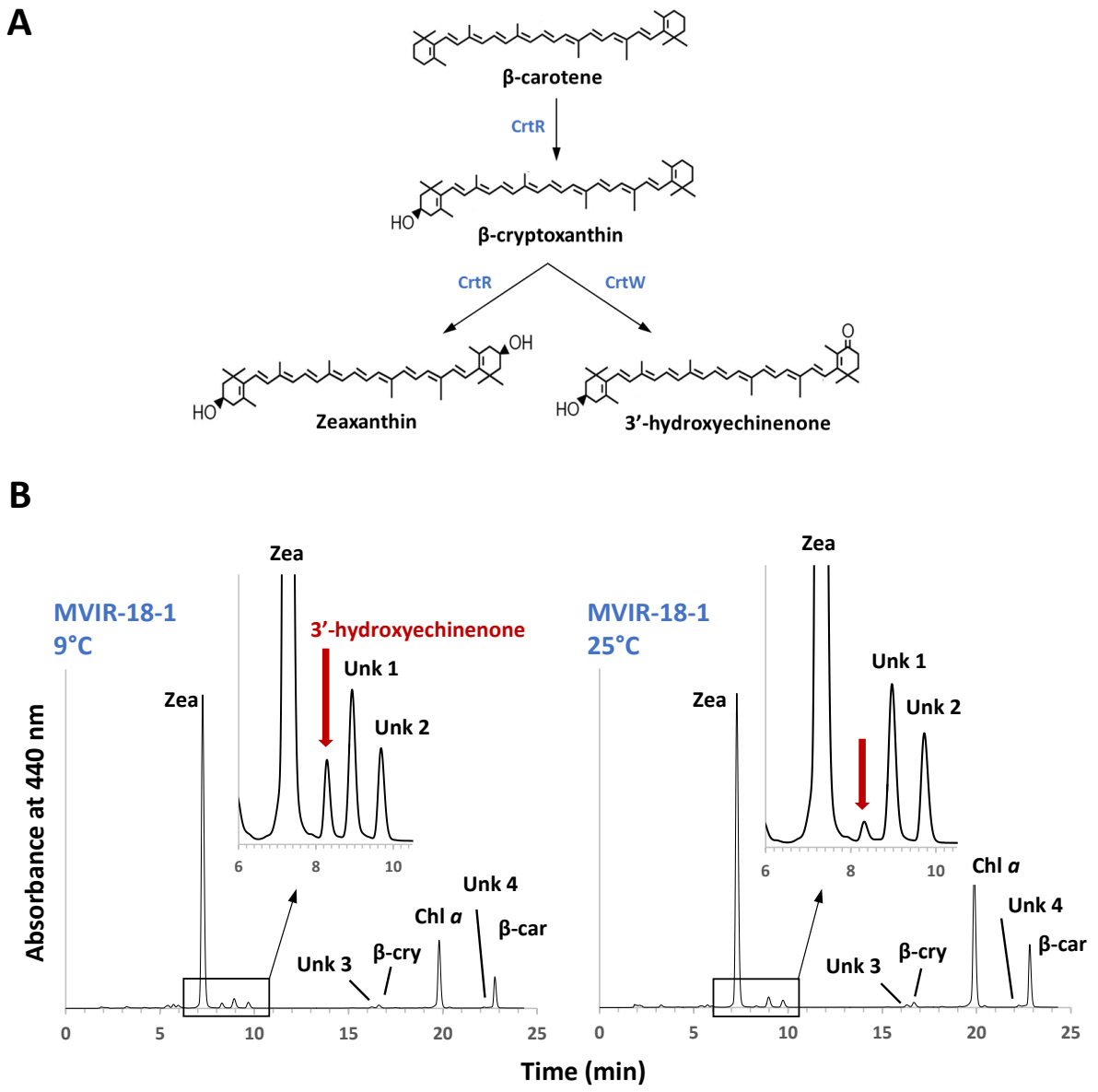

Figure S11: Possible biosynthesis pathway of zeaxanthin and 3'-hydroxyechinenone from β-carotene in marine *Synechococcus* (**A**). High pressure liquid chromatography analysis of membrane pigments showing the 3'-hydroxyechinenone peak (red arrow), in the subpolar *Synechococcus* sp. MVIR-18-1 grown at two extreme temperatures of the thermal *preferendum* (**B**). **β-car**: β-β-carotene; **β-cry**: β-β-cryptoxanthin; **Unk**: unknown xanthophyll; **Zea**: zeaxanthin.

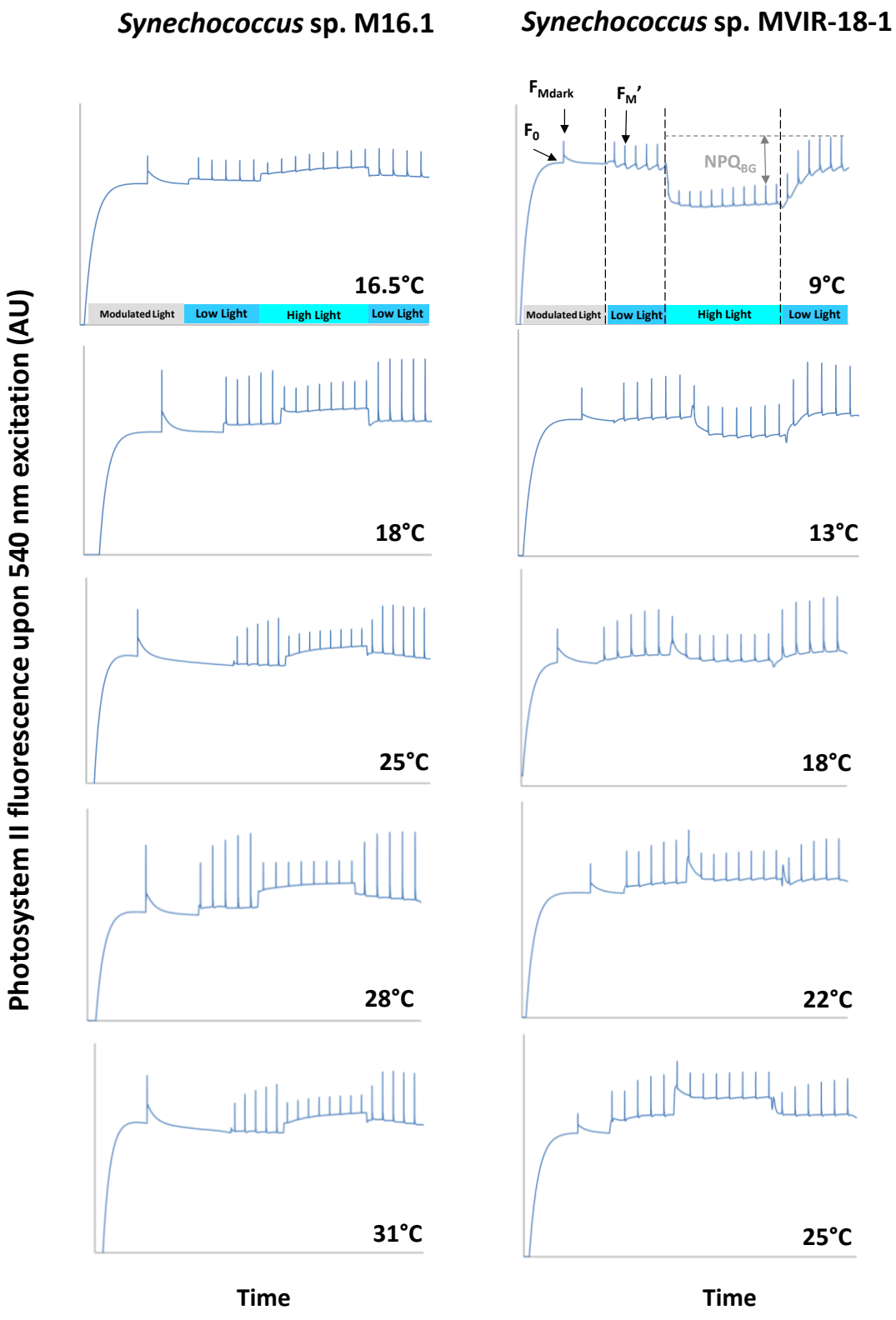

Figure S12: Examples of fluorescence traces recorded to study non photochemical quenching of fluorescence induced by high blue-green (480 nm) irradiance (NPQ_{BG}), in *Synechococcus* spp. M16.1 (left panel) and MVIR-18-1 (right panel), grown over their thermal *preferendum* . The different fluorescence levels are shown on MBIR-18-1 _9°C, the case showing maximal NPQ_{BG} in our experimental conditions. For a review see e.g. (9).

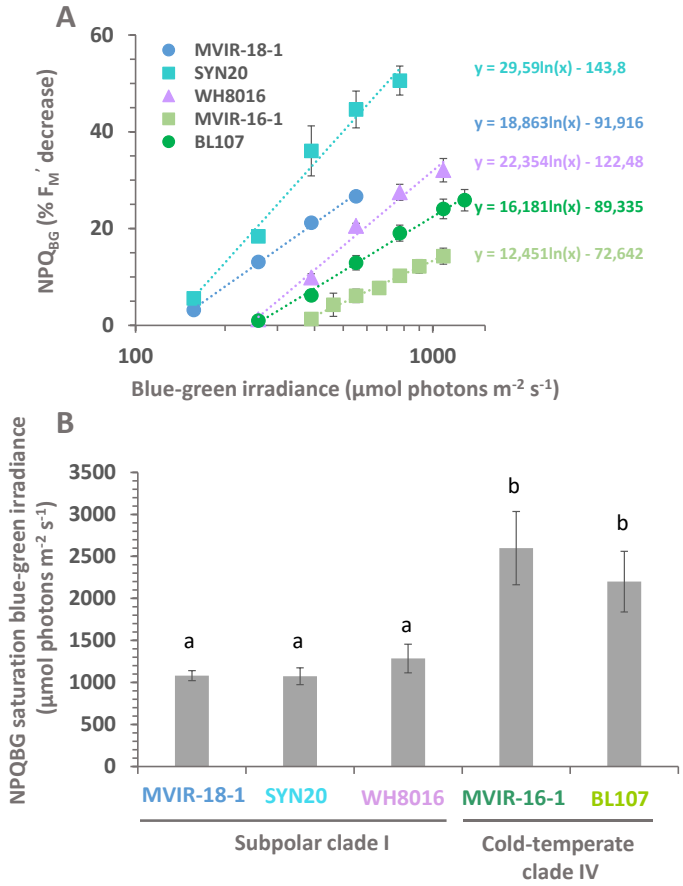

Figure S13: Ln-transformed irradiance response curves (**A**) and estimated saturation irradiances (**B**) of non-photochemical quenching of fluorescence induced by blue-green light (480 nm; NPQ_{BG}) for five cold-adapted strains of marine *Synechococcus* belonging to the cold-adapted clades I and IV (Kruskal-Wallis, *df*=3, *p*-value<0.05).

Section 2: Molecular characteristics of marine *Synechococcus* OCPs

Table S2: Accession numbers of sequences used to build the phylogenetic analysis of marine *Synechococcus* OCPs (cluster CK_00001790 in Cyanorak). Sequences from the Ocean Gene Atlas (OGA) were downloaded on the OGA website (10) and identified by their number in the Reference Gene Catalog database (OM-RGC; (11)).

	Sequence name	Origin	Clade	Accession
01	MVIR-18-1	MVIR-18-1 genome	I	CP047942
02	SYN20	SYN20 genome	I	CP047959
03	ROS8604	ROS8604 genome	I	CP047946
04	WH8016	WH8016 genome	I	AGIK00000000.1
05	CC9311	CC9311 genome	I	CP000435
06	WH8020	WH8020 genome	I	CP011941
07	PROS-9-1	PROS-9-1 genome	I	CP047961
08	UW179B	Lee et al. 2019	I	WP_115070113.1
09	MEDG-68	MEDG-68 metagenome	I	QOPS01000005
10	AG-686-F08	Metagenome	I	GCA_003210315.1
11	NP17	TARA Ocean	I	MBT66467.1
12	7340373	OGA, TARA Ocean	I	OM-RGC.v2.007340373
13	7307333	OGA, TARA Ocean	I	OM-RGC.v2.007307333
14	7454275	OGA, TARA Ocean	I	OM-RGC.v2.007454275
15	7325291	OGA, TARA Ocean	I	OM-RGC.v2.007325291
16	M16.1	M16.1 genome	II	CP047954

17	A15-44	A15-44 genome	II	CP047938
18	RS9907	RS9907 genome	II	CP047944
19	PROS-U-1	PROS-U-1 genome	II	CP047951
20	HB1133	HB1133 genome	II	SDBW00000000
21	UW86	Lee et al. 2019	II	WP_115161908.1
22	MED650	TARA Ocean	II	MAI95430.1
23	AG-673-B08	Metagenome	II	GCA_003209035.1
24	SAT82	TARA Ocean	II	MAX88342.1
25	UW69	Lee et al. 2019	II	WP_115021825.1
26	BS307-5m-G38	Cabello-Yeves et al. 2020	II	MBL6801897.1
27	7305616	OGA, TARA Ocean	II	OM-RGC.v2.007305616
28	7319027	OGA, TARA Ocean	II	OM-RGC.v2.007319027
29	7698709	OGA, TARA Ocean	II	OM-RGC.v2.007698709
30	BOUM118	BOUM118 genome	III	CP047947
31	WH8103	WH8103 genome	III	LN847356.1
32	WH8102	WH8102 genome	III	BX548020
33	RS9915	RS9915 genome	III	CP047934
34	A15-28	A15-28 genome	III	CP047931
35	A15-24	A15-24 genome	III	CP047960
36	A18-40	A18-40 genome	III	CP047956
37	A18-46.1	A18-46.1 genome	III	CP047955
38	MED-G133	MED-G133 metagenome	III	SHBS01000037
39	YX04-3	Zheng et al. 2020	III	RNC93067.1
40	7305562	OGA, TARA Ocean	III	OM-RGC.v2.007305562
41	7306351	OGA, TARA Ocean	III	OM-RGC.v2.007306351
42	BL107	BL107 genome	IV	AATZ00000000
43	CC9902	CC9902 genome	IV	CP000097
44	MED-G69	MED-G69 metagenome	IV	RCL56366.1
45	AG-683-C23	Metagenome	IV	GCA_003208835.1
46	5897902	OGA, TARA Ocean	IV	OM-RGC.v2.005897902
47	7305455	OGA, TARA Ocean	IV	OM-RGC.v2.007305455
48	6955513	OGA, TARA Ocean	IV	OM-RGC.v2.006955513
49	7344225	OGA, TARA Ocean	IV	OM-RGC.v2.007344225
50	WH7803	WH7803 genome	V/VI	CT971583
51	WH7805	WH7805 genome	V/VI	AAOK00000000
52	BMK-MC-1	BMK-MC-1 genome	V/VI	CP047939
53	PROS-7-1	PROS-7-1 genome	V/VI	CP047945
54	MEDNS5	MEDNS5 genome	V/VI	CP047952
55	TMED90	TARA Ocean	V/VI	OUX72510.1
56	BS301-5m-G53	Cabello-Yeves et al. 2020	V/VI	MBL6742682.1
57	RS9917	RS9917 genome	VIII	AANP00000000
58	RS9909	RS9909 genome	VIII	CP047943
59	WH8101	WH8101 genome	VIII	CP047932
60	BS55D	BS55D genome	VIII	PHQT00000000
61	BS56D	BS56D genome	VIII	PHQU00000000
62	ARS1019	TARA Ocean	VIII	ASM269032v1
63	7312865	OGA, TARA Ocean	VIII	OM-RGC.v2.007312865
64	A15-127	A15-127 genome	WPC1	CP047948
65	KORDI-49	KORDI-49 genome	WPC1	CP006270.1
66	7306326	OGA, TARA Ocean	WPC1	OM-RGC.v2.007306326
67	7342442	OGA, TARA Ocean	WPC1	OM-RGC.v2.007342442
68	RCC307	RCC307 genome	5.3	CT978603
69	TMED185	TARA Ocean	5.3	OUW39040.1
70	7305569	OGA, TARA Ocean	5.3	OM-RGC.v2.007305569

Structural functionalities of marine OCPs

Hereafter we use the amino acid numeration of *Synechocystis* sp. PCC 6803 strain, in order to facilitate comparison with previous studies. In the inactive orange conformation, the two domains form a globular protein whose conformation is notably maintained by a salt bridge arginine (R155) - glutamate (E244) in the middle of the protein. The bridge is conserved in all marine *Synechococcus* OCPs, with the difference that the negative charge is brought by an aspartate (S244) residue. The residues tyrosine Y201 and tryptophan W288, tyrosine Y44 and tryptophan W101, respectively involved in H-bonds with the keto-group and in Pi interactions with the hydroxyl group of the xanthophyll, are also well conserved in marine OCPs. The active red conformation of freshwater OCPs is notably maintained by the residues glutamate E34, proline P126 and tyrosine Y129. They are all conserved in marine OCPs, except that E34 can be replaced by a smaller aspartate D34 residue only in strains of the subpolar *Synechococcus* clade I. This is interesting because mutating this residue in *Synechocystis* sp. PCC 6803 has been shown to have a direct impact on the fluorescence quenching efficiency of the red conformation (12). Are also conserved the arginine R155 residue involved in the fixation to the phycobilisome, the glutamate E174 and the arginine R185 allowing the conformation back conversion, and the aspartate residue D220 interacting with the fluorescence recovery protein, which catalyzes the OCP back conversion. The other residue shown to be involved in this interaction, the phenylalanine F299, is replaced by a tyrosine in all marine *Synechococcus* OCPs. This globally suggests that the global OCP photocycle mechanism is well conserved in marine *Synechococcus*.

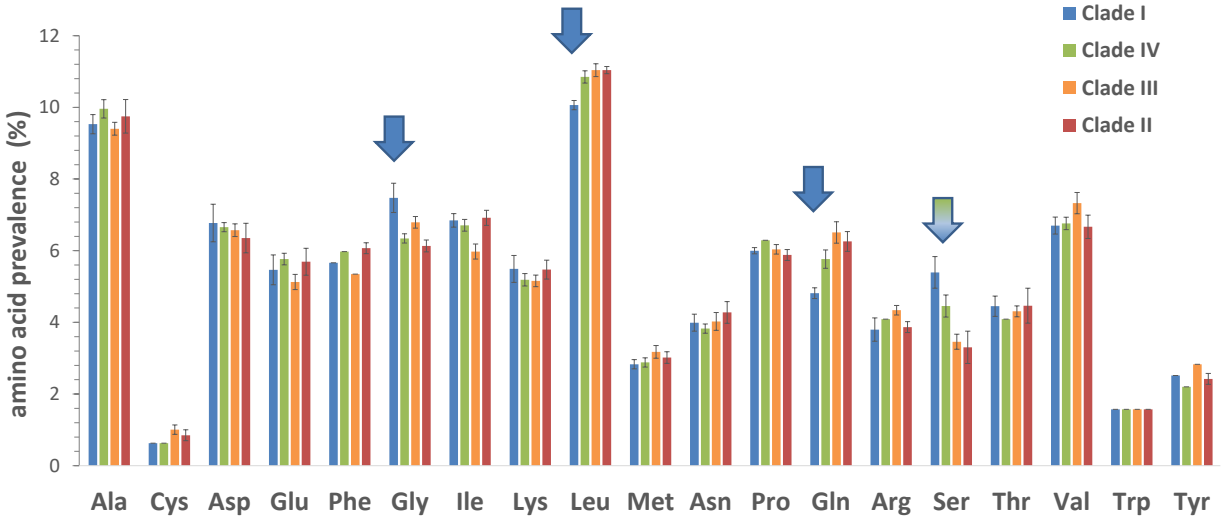

Figure S14: Relative composition in amino acid of the Orange Carotenoid Protein of marine *Synechococcus* thermotypes, including the subpolar clade I (11 sequences), the cold temperate clade IV (6 sequences), the warm temperate clade III (9 sequences) and the tropical clade II (11 sequences). There is no histidine in the protein. The arrows show the specific differences of clade I OCP sequences (blue) and of both clades I and IV (blue-green).

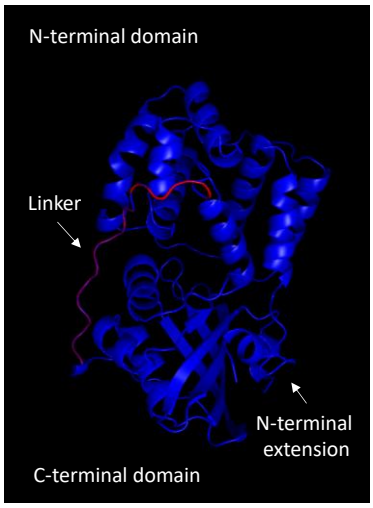

Figure S15: Differential structure model of the OCP of the subpolar MVIR-18-1 (blue) and the tropical M16.1 (red) *Synechococcus* strains. When the conformation is identical between the two superimposed protein structures, the MVIR-18-1 (blue) is shown. When there is a difference, both the subpolar and the tropical structures are shown. Note that the linker region appears to be the most different between the two OCPs.

Section 3: Metagenomics of *ocp* genes of marine *Synechococcus*

Table S3: Localization, seawater temperature and *petB* gene normalized counts of the sampling stations of the TARA expeditions (TARA Ocean and TARA Arctic) studied in this work.

TARA station #	Latitude	Longitude	Temperature (°C)	*petB* gene
4	36.6	-6.6	20.2	634.6
9	39.2	5.9	24.5	1322.3
23	42.2	17.7	17.2	759.6
25	39.4	19.4	18.3	2600.8
30	33.9	32.9	20.4	185.0
31	27.2	34.8	25.0	728.8
33	21.9	38.3	27.3	5215.8
34	18.4	39.9	27.6	3172.5
36	20.8	63.5	25.7	2578.9
38	19.0	64.5	26.3	3295.2
41	14.6	70.0	29.2	394.4
42	6.0	73.9	30.1	68.4
45	0.0	71.6	30.6	226.6
56	-15.3	43.3	27.3	153.0
57	-17.0	42.7	26.6	4483.6
62	-22.3	40.3	25.1	843.3
64	-29.5	38.0	22.2	820.6
65	-35.2	26.3	21.8	936.2
66	-34.9	17.9	15.0	125.1
67	-32.2	17.7	13.0	489.2
68	-31.0	4.7	16.9	2130.7
76	-20.9	-35.2	23.4	184.0
78	-30.1	-43.3	20.1	619.4
80	-40.7	-52.2	19.3	488.9
81	-44.5	-52.5	13.9	724.7
82	-47.2	-58.3	7.6	8.5
83	-54.4	-65.0	7.4	5.3
84	-60.2	-60.6	1.9	0
89	-57.7	-67.0	5.8	2.3
93	-34.1	-73.1	18.1	2381.0

123	-8.9	-140.5	26.6	1629.0
124	-9.2	-140.5	26.6	4412.9
140	7.4	-79.3	26.6	2529.8
141	9.8	-80.0	27.2	6831.4
145	39.2	-70.0	14.0	807.7
146	34.7	-71.3	19.3	887.3
148	31.7	-64.2	20.5	2034.5
149	34.1	-49.9	18.8	1088.2
150	35.9	-37.3	17.6	586.8
152	43.7	-16.8	14.3	1161.4
155	54.5	-16.8	11.1	538.8
210	61.5	-56.0	5.4	59.4

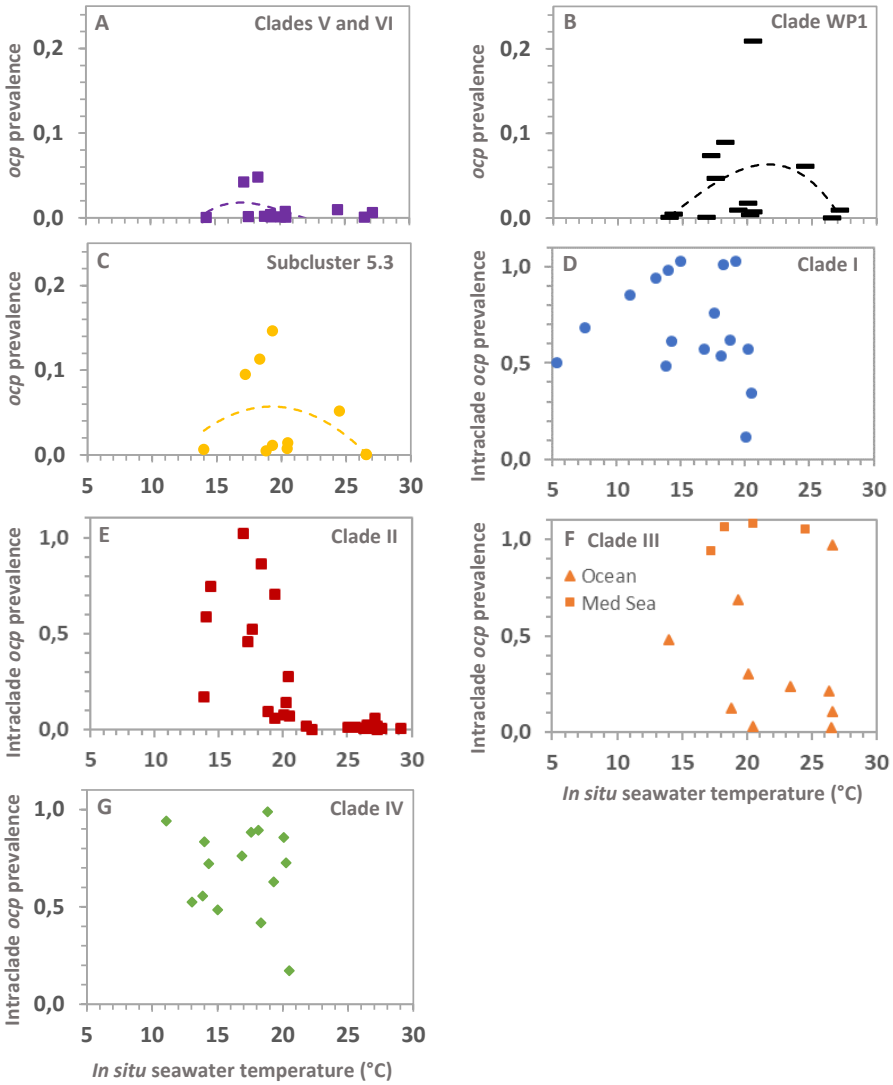

Figure S16: Prevalence of the *ocp* gene variants of the minor *Synechococcus* clades, function of seawater temperature (**A**, **B** and **C**). The values ≥ 0.1 are Mediterranean Sea stations. Intraclade prevalence of the *ocp* gene for th four major Synechococcus clades I (**D**), II (**E**), III (**F**) and IV (**G**)

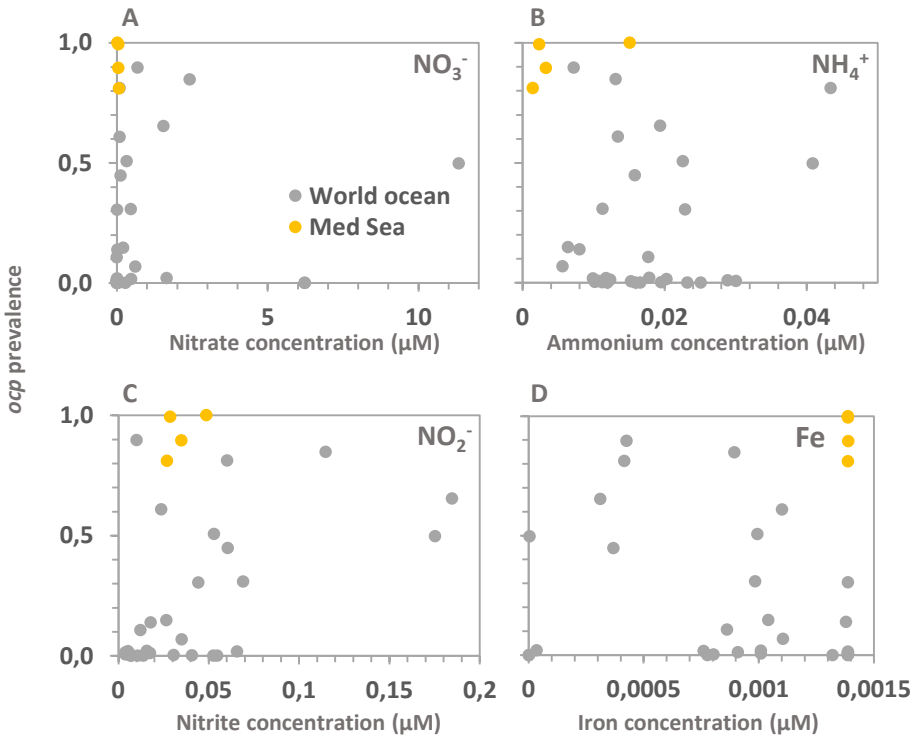

Figure S17: Prevalence of the *ocp* gene variants for all *Synechococcus* clades function of the concentration of nitrate (A), ammonium (B), nitrite (C) and iron (D) in seawater.

Section 4: Metabolic cost of thermal photophysiological acclimation

Dataset S1 (separate spreadsheet file): Study of the metabolic cost of thermoacclimation for major pigmented protein complexes, in the two *Synechococcus* temperature ecotypes M16.1 (tropical) and MVIR-18-1 (subpolar).

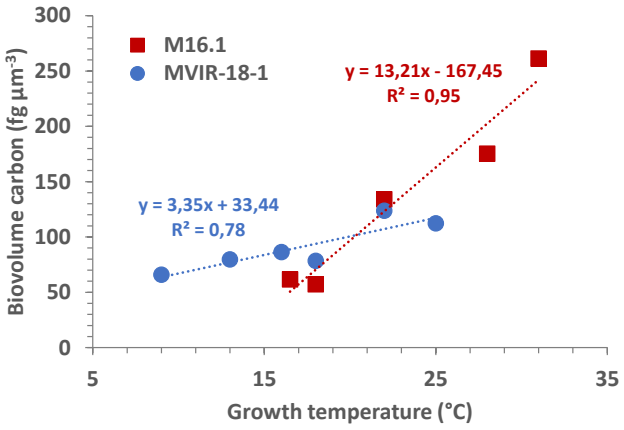

Figure S18: Allocation in carbon to photosynthetic pigmented complexes (phycobilisome, photosystem reaction centers and orange carotenoid protein) function of growth temperature, in *Synechococcus* spp. M16.1 (red) and MVIR-18-1 (blue).

References

1. S. Mazard, M. Ostrowski, F. Partensky, D. J. Scanlan, Multi-locus sequence analysis, taxonomic resolution and biogeography of marine *Synechococcus*. *Environ. Microbiol.* **14**, 372–386 (2012).
2. G. K. Farrant, *et al.*, Delineating ecologically significant taxonomic units from global patterns of marine picocyanobacteria. *Proc. Natl. Acad. Sci. U. S. A.* **113**, E3365–E3374 (2016).
3. H. Doré, *et al.*, Evolutionary Mechanisms of Long-Term Genome Diversification Associated With Niche Partitioning in Marine Picocyanobacteria. *Front. Microbiol.* **11**, 1–23 (2020).
4. J. Pittera, *et al.*, Connecting thermal physiology and latitudinal niche partitioning in marine *Synechococcus*. *ISME J.* **8**, 1–14 (2014).
5. C. Six, *et al.*, Diversity and evolution of phycobilisomes in marine *Synechococcus* spp.: a comparative genomics study. *Genome Biol.* **8**, R259 (2007).
6. F. Humily, *et al.*, A Gene Island with Two Possible Configurations Is Involved in Chromatic Acclimation in Marine *Synechococcus*. *PLoS One* **8**, e84459 (2013).
7. T. Platt, C. L. Gallegos, Modelling Primary Production. In: Falkowski P.G. (eds) Primary Productivity in the Sea. Environmental Science Research, vol 19. Springer, Boston, MA. https://doi.org/10.1007/978-1-4684-3890-1_19 (1980).
8. L. J. Ong, A. N. Glazer, Phycoerythrins of marine unicellular cyanobacteria: I. Bilin types and locations and energy transfer pathways in *Synechococcus* spp. phycoerythrins. *J. Biol. Chem.* **266**, 9515–9527 (1991).
9. D. Kirilovsky, Photoprotection in cyanobacteria: the orange carotenoid protein (OCP)-related non-photochemical-quenching mechanism. *Photosynth. Res.* **93**, 7–16 (2007).
10. E. Villar, T. Vannier, C. Vernette, M. Lescot, M. Cuenca, A. Alexandre, P. Bachelerie, T. Rosnet, E. Pelletier, S. Sunagawa, P. Hingamp. The Ocean Gene Atlas: exploring the biogeography of plankton genes online. Nucleic Acids Research doi: 10.1093/nar/gky376 (2018).
11. S. Sunagawa *et al.*, Structure and Function of the Global Ocean Microbiome. Science **348**, 1261359-1261359 (2015).
12. R. L. Leverenz, *et al.*, A 12 Å carotenoid translocation in a photoswitch associated with cyanobacterial photoprotection. Science **348**, 1463–1466 (2015).